CANCER

Engineered extracellular vesicles with DR5 agonistic scFvs simultaneously target tumor and immunosuppressive stromal cells

Yeye Guo[1,2], Huaishan Wang[1], Shujing Liu[1], Xiaogang Zhang[1], Xingyue Zhu[1], Lili Huang[1], Wenqun Zhong[3], Lei Guan[3], Yeqing Chen[4], Min Xiao[4], Lingling Ou[1], Jingbo Yang[3], Xiang Chen[2], Alexander C. Huang[5], Tara Mitchell[5], Ravi Amaravadi[5], Giorgos Karakousis[6], John Miura[6], Lynn Schuchter[5], Ahron Flowers[5], Qiuxian Zheng[4], Haiwei Mou[4], Phyllis Gimotty[7], Meenhard Herlyn[4], Wei Guo[3], Xiaowei Xu[1]*

Small extracellular vesicles (sEVs) are nanosized vesicles. Death receptor 5 (DR5) mediates extrinsic apoptosis. We engineer DR5 agonistic single-chain variable fragment (scFv) expression on the surface of sEVs derived from natural killer cells. PDGFR transmembrane domain delivers DR5-scFvs to the surface of sEVs. DR5-scFv sEVs rapidly induce apoptosis of different types of DR5$^+$ cancer cells, myeloid-derived suppressor cells (MDSCs), and cancer-associated fibroblasts (CAFs). DR5-scFv sEVs migrate specifically to DR5$^+$ tumors in vitro and in vivo. Systemic delivery of DR5-scFv sEVs significantly inhibits the growth of DR5$^+$ melanoma, liver cancer, and breast cancer and prolongs mouse life span without significant toxicity. DR5-scFv sEVs are significantly more efficacious than DR5 antibodies in vivo. In organotypic patient-derived melanoma slice cultures, DR5-scFv sEVs effectively inhibit melanoma cells and MDSCs and activate CD8$^+$ T cells. Our studies demonstrate that DR5-scFv sEVs can inhibit tumor growth by targeting tumor cells and immunosuppressive stromal cells in the TME.

INTRODUCTION

Chimeric Antigen Receptor (CAR)–T cell therapies have revolutionized the treatment of hematopoietic malignancies. However, their efficacy in treating solid cancers is questionable (*1*). Major barriers to effective CAR-T cell therapy in solid cancers include the limited infiltration of CAR-T cells into the tumor, a hostile tumor microenvironment (TME), and T cell exhaustion (*2*). In addition, unlike hematological malignancies, in which the cancer cells commonly express specific surface markers, solid tumors express tumor-associated antigens, which are also expressed at a lower level in normal tissues. The risk of on-target off-tumor toxicity is high, as illustrated by the catastrophic toxicity in Her2-CAR T cell (*3*) and GD2-CAR T cell (*4*) clinical trials. A clear unmet clinical need exists for better cellular therapies for solid tumors.

Small extracellular vesicles (sEVs) are nanosized vesicles that are relatively stable in body fluid and can cross biological barriers to reach specific sites (*5*, *6*). sEVs carry many characteristics of their parental cells and show outstanding biocompatibility. sEVs from cytotoxic immune cells, such as natural killer (NK) cells, CD8$^+$ T cells, and γδ T cells, carry perforin, lysozymes, and other cytotoxic molecules to cancer cells (*7*–*9*). However, sEVs from unmodified immune cells lack the tumor-targeting ability (*10*). sEVs released by CAR-T cells have CAR on their surface, and they have shown promising targeting and treatment efficacy against certain cancers in preclinical models (*11*, *12*).

Death receptor 5 (DR5) is a receptor for tumor necrosis factor–related apoptosis-inducing ligand (TRAIL). DR5 is highly expressed in many types of cancer, such as liver cancer, melanoma, and pancreatic cancer, but significantly less in normal tissues (*13*–*15*). DR5 is also highly expressed in myeloid-derived suppressor cells (MDSCs), major immunosuppressive cells in the TME. DR5 activation induces apoptosis, and DR5 and related death receptors are attractive targets for cancer therapy (*16*). Several DR5 agonistic antibodies have been evaluated clinically (*17*–*20*). DR5 agonistic antibodies significantly decreased MDSCs in patients' tumors and circulation (*21*). Although cancer patients tolerate these antibodies well, tumor shrinkage in the treated cancer patients was rarely observed.

NK cells are innate immune cells that potently kill tumor cells (*22*). The NK cell line NK92 has been well characterized and used in clinical trials because of its safety profile (*23*, *24*). NK92 cells belong to the CD56^{bright} NK subset and secrete numerous immune regulatory factors, including interferon-γ (IFN-γ) and tumor necrosis factor–α (TNF-α). sEVs from NK92 cells have been reported to contain cytotoxic proteins and exert antitumor effects. When injected intratumorally, sEVs from NK92 cells inhibited mouse B16F10 melanoma in vivo (*25*).

Here, we engineered NK92 cells to secrete sEVs with DR5 agonistic scFvs on the surface. Platelet-derived growth factor receptor (PDGFR) transmembrane domain (TM) delivers more DR5-scFvs to the surface of sEVs than CD8 TM. Live cell imaging studies showed that DR5-scFv sEVs rapidly induced apoptosis of DR5$^+$ melanoma cells. The engineered sEVs specifically migrated to DR5$^+$ melanoma cells in vitro and in vivo. Systemic delivery of DR5-scFv sEVs significantly inhibited the growth of multiple cancer types and prolonged the life span of treated mice. Adverse reactions in the treated mice were not observed. DR5-scFv sEVs are significantly more cytotoxic to DR5$^+$ cancer cells than DR5 antibodies in vitro and in vivo. Furthermore, DR5-scFv sEVs significantly inhibited MDSCs and

[1]Department of Pathology and Laboratory Medicine, Perelman School of Medicine, University of Pennsylvania, Philadelphia, PA 19104, USA. [2]Department of Dermatology, Xiangya Hospital, Central South University, Changsha 41000, China. [3]Department of Biology, University of Pennsylvania, Philadelphia, PA 19104, USA. [4]Molecular and Cellular Oncogenesis Program, The Wistar Institute, Philadelphia, PA 19104, USA. [5]Department of Medicine and Abramson Cancer Center, University of Pennsylvania, Philadelphia, PA 19104, USA. [6]Department of Surgery, University of Pennsylvania, Philadelphia, PA 19104, USA. [7]Department of Biostatistics, University of Pennsylvania, Philadelphia, PA 19104, USA.
*Corresponding author. Email: xug@pennmedicine.upenn.edu

cancer-associated fibroblasts (CAFs) in the TME and activated CD8$^+$ T cells in organotypic patient-derived melanoma slice culture models. Together, DR5-scFv sEVs inhibit tumor growth by targeting tumor cells and immunosuppressive stromal cells in the TME.

RESULTS

DR5-scFv CAR-T cells inhibit melanoma growth in vivo when administered intratumorally but not systemically

DR5 is highly expressed in cancer cells such as liver, melanoma, and pancreatic cancer (fig. S1). We measured the expression of DR5 in melanoma cells (A375, A2058, SK-Mel-28, and UACC-903), keratinocytes (HaCaT), and fibroblasts (BJ). Immortalized noncancerous cell lines, HaCaT and BJ cells, expressed lower DR5 levels than melanoma cells (Fig. 1A). Furthermore, in situ hybridization confirmed the expression of DR5 in melanoma but not in normal skin (Fig. 1B). We designed second-generation CARs targeting DR5, taking advantage of DR5-scFv sequences obtained from the International Immunogenetics Information System (IMGT). The DR5–4-1BBz–CAR lentiviral vectors expressed DR5 agnostic scFv, a CD8 TM, the costimulatory domain of 4-1BB, and the T cell activating domain CD3ζ (Fig. 1C). DR5-scFv CAR was cloned into the pTRPE lentiviral vector and confirmed by Sanger sequencing. T cells from freshly collected human peripheral blood mononuclear cells (PBMCs) were expanded and transfected with lentiviruses carrying the DR5 CAR constructs (fig. S2). DR5$^+$ A375 melanoma cells were injected into the flanks of nude mice. When the

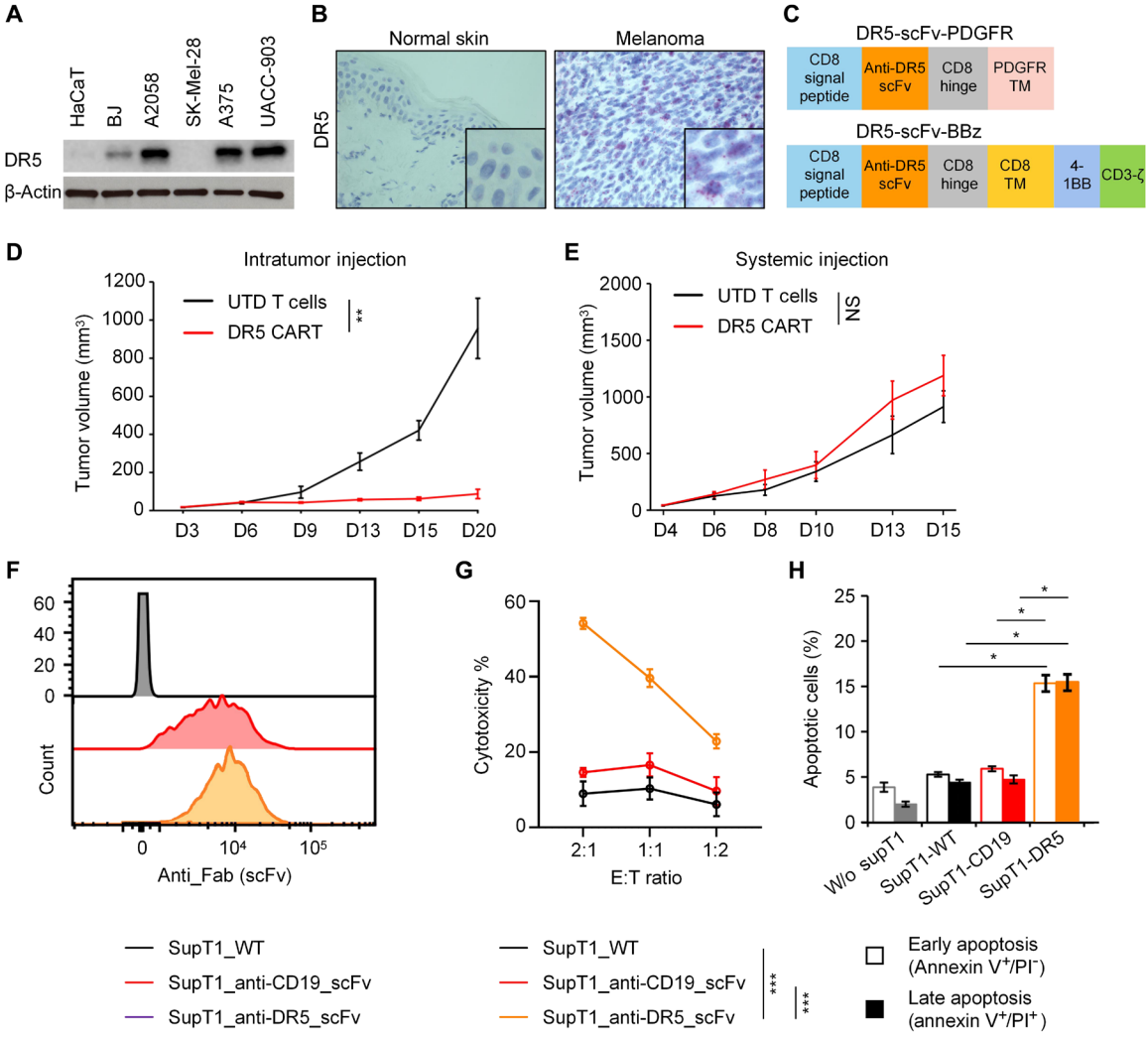

Fig. 1. DR5-scFvs induce apoptosis of DR5$^+$ tumor cells. (**A**) Expression of DR5 in different cell types. Proteins were extracted from different cells and subjected to immunoblot analysis using antibodies against DR5. (**B**) DR5 is highly expressed in melanoma cells. The expression of DR5 mRNA in normal skin (left panel) and melanoma (right panel) was detected using in situ hybridization. (**C**) Schematic representation of DR5–4-1BBz CAR and DR5-PDGFR lentiviral vectors. (**D** and **E**) Effect of DR5 CAR-T cells on tumors in vivo. Melanoma xenografts were established by subcutaneous injection of A375 cells into the right flank of nude mice ($n = 5$). Untransfected T (UTD) cells or DR5-scFv CAR-T cells (2.5×10^6 per injection) were injected into the mice through intratumor injection (D) or tail vein injection (E). $^{**}P < 0.01$. (**F**) CAR scFv expression in transfected SupT1 cells. SupT1 cells were transfected with CD19-CAR or DR5-CAR lentiviral vectors. The expression of CD19-scFvs or DR5-scFv in SupT1 cells was detected using flow cytometry. (**G**) Luciferase-killing assay of DR5-CAR SupT1 cells or CD19-CAR SupT1 cells in A375 cells. A375 cells were treated with DR5-CAR SupT1 cells or CD19-CAR SupT1 at the indicated ratio of effector cells to target cells (E:T ratio). $^{***}P < 0.001$. (**H**) DR5-CAR SupT1 cells induce apoptosis in A375 cells. A375 cells treated with wild-type (WT), CD19-CAR, or DR5-CAR transfected SupT1 cells were subjected to annexin V–fluorescein isothiocyanate (FITC)/PI staining. Data are presented as means ± SD ($n = 3$). $^*P < 0.05$.

tumors became palpable, these mice were treated with DR5-scFv CAR-T cells via intratumoral or tail vein injection. DR5 CAR-T cells produced significant tumor growth inhibition in A375 melanoma xenografts when injected intratumorally (Fig. 1D). However, systemic infusion of DR5 CAR-T cells produced no significant tumor growth inhibition (Fig. 1E), and histology showed no infiltrating $CD3^+$ T cells in the tumors.

Since DR5 agonistic antibodies are known to induce tumor cell apoptosis, we studied whether the DR5-scFv CAR can directly induce apoptosis of $DR5^+$ cells. Lymphoblastic leukemia SupT1 cells lack cytolytic activity (*26*). We generated stable DR5 CAR-expressing SupT1 cells and confirmed the expression of DR5-CAR on the cell surface (Fig. 1F). CD19-CAR was used as a control. DR5-CAR SupT1 cells effectively killed A375 melanoma cells in a dose-dependent manner, whereas CD19-CAR SupT1 cells showed little effect (approximately 10 to 20% killing efficiency; Fig. 1G). Annexin V and PI stains showed that DR5-CAR SupT1 cells induced apoptosis of A375 melanoma cells (Fig. 1H). These results indicate that DR5 agonistic scFvs are directly cytotoxic to target cells.

PDGFR TM delivers more DR5-scFvs to the surface of sEVs than CD8 TM

Since sEVs are significantly smaller than T cells and can readily enter the TME (*27*, *28*), we postulate that sEVs carrying DR5-scFvs may be an alternative therapy for CAR-T cells for solid tumors. To deliver more DR5-scFvs to the surface of sEVs, we utilized the PDGFR-TM, which has been demonstrated to increase the membrane expression of targeting peptides (*29*). We replaced the CD8 TM of DR5–4-1BBz–CAR with PDGFR-TM domains and removed the 4-1BB and CD3ζ domains (Fig. 1C). DR5-PDGFR constructs with four different DR5-scFvs from DR5 were generated. NK92 cells were transfected with these DR5-PDGFR plasmids. Only NK92 cells transfected with the DR5-PDGFR plasmids containing scFv from tigatuzumab expanded well in vitro. NK92 cells transfected with the other three plasmids did not proliferate well (fig. S3). sEVs from NK92 cells transfected with DR5-PDGFR and DR5–4-1BBz–CAR with scFvs from tigatuzumab were further studied. Transfected cells were sorted by fluorescence-activated cell sorting (FACS) (Fig. 2A). The cell proliferation assay showed that transfection with either DR5-PDGFR or DR5–4-1BBz–CAR did not affect NK92 cell proliferation (Fig. 2B).

sEVs secreted by the transfected and control NK92 cells were determined by nanoparticle tracking analysis (NTA) using NanoSight NS300. The diameters of sEVs were approximately 80 to 90 nm, and no significant difference was observed among the three groups (Fig. 2, C and D). Western blot analysis showed that sEVs were positive for EV markers, including CD9, CD81, and TSG101, but negative for the endoplasmic reticulum protein calnexin (Fig. 2E). Next, we compared the surface expression of DR5-scFvs in sEVs by immunoelectron gold labeling. More gold particles were detected on the surface of sEVs derived from DR5-PDGFR-NK92 cells than DR5–4-1BBz–NK92 cells. Gold particles were not detected on EVs derived from the control NK92 cells (Fig. 2F). On-bead flow cytometry analysis showed that approximately 50% more sEVs secreted by DR5-PDGFR-NK92 cells (DR5-scFv sEVs) had detectable DR5-scFvs than sEVs from DR5–4-1BBz–NK92 cells (Fig. 2G and fig. S4). These data demonstrate that the PDGFR TM is superior to CD8 TM in delivering DR5-scFv to the surface of sEVs.

DR5-scFv sEVs specifically kill $DR5^+$ cells

To determine the specificity of DR5-scFv sEVs, melanoma cells were treated with phosphate-buffered saline (PBS) (−) or 2.5, 5, and 10 μg of sEVs from DR5–4-1BBz–NK92 or DR5-PDGFR-NK92 cells. DR5-scFv sEV treatment preferentially produced cytotoxicity in cells with high DR5 expression, such as A2058, UACC-903, and A375 (Fig. 3, A to C). In contrast, cells with lower or no-detectable DR5 expression, such as BJ, HaCaT, and SK-Mel-28 cells, were less vulnerable to the killing by DR5-scFv sEVs (Fig. 3, D to F). The direct cytotoxicity of DR5-scFv sEVs was also visualized using live cell imaging. A375–green fluorescent protein (GFP)–firefly Luciferase (ffLuc) cells were labeled with propidium iodide (PI) (red) and Hoechst 33342 (blue), and DR5-scFv sEVs were labeled with deep red. Melanoma cells were treated with sEVs for 3 hours (movie S1). Membrane blebbing occurred rapidly in some of the tumor cells, and these cells turned red, indicative of cell death (Fig. 3G and movie S1). sEVs from control NK92 cells were also cytotoxic to tumor cells, but their tumor killing was not correlated with target cells' DR5 expression. Besides melanoma, DR5 is highly expressed in Huh-7, a human liver cancer cell line, and OVCAR-5, a human ovarian cancer cell line. In contrast, MDA-MB-231, a human breast cancer cell line, and PANC-1, a pancreatic cancer cell line, showed relatively lower DR5 expression (Fig. 3H). These cancer cells were treated with DR5-scFv sEVs, and the results showed that DR5-scFv EVs more effectively killed $DR5^{high}$ cells (Huh-7 and OVCAR-5) than $DR5^{low}$ cells (MDA-MB-231 and PANC-1) (Fig. 3, I to L). sEVs from DR5-PDGFR-NK92 cells generally showed the highest cytotoxicity to cancer cells, supporting that the number of DR5 agonistic scFv moieties on the surface of sEVs correlates with cytotoxicity.

To compare the effect of targeting DR5 with other tumor-associated antigens, we constructed HER2-PDGFR plasmids with the same backbone as the DR5-PDGFR plasmids. sEVs from NK92 cells transfected with HER2-PDGFR did not have the same cytotoxicity to A375 melanoma cells as the DR5-scFv sEVs (fig. S5A). Furthermore, dual staining with Hoechst 33342/PI demonstrated that sEVs derived from DR5-CAR SupT1 and DR5-CAR 293T cells induced cell death in A375 cells. However, sEVs derived from CD19-CAR SupT1 cells or CD19-CAR 293T cells could not exert a cytotoxic effect (fig. S5, B and C). These results further support that DR5 agonistic scFvs in the sEVs can directly induce target cell death.

Next, we compared the protein contents of NK92 cells and sEVs from these cells using the reverse-phase protein array (RPPA), which profiled 491 proteins in various cellular pathways. Component analyses showed that protein expression in NK92 cells was uniform in different batches of cells. In contrast, protein expression in sEVs from these cells was varied, suggesting that protein packaging into sEVs is a relatively random process (fig. S6A). Nevertheless, all 491 proteins were detectable in both cells and sEVs, and the expression levels of approximately one-third of the proteins between cells and sEVs were similar. Volcano plots showed that NK92-sEVs were enriched in apoptosis/necrosis inducers such as NDRG1, RIPK3, and ATM (fig. S6B). Many apoptosis/necrosis inducers such as caspase-3 (CASP3), Bim (BCL2L11), and Bid were detected in both NK92-sEVs and NK92 cells (Fig. 3M), supporting that cytotoxic molecules are present in the sEVs from NK92 cells.

DR5-scFv sEVs are more effective in tumor killing than DR5 antibodies

We next compared the cytotoxicity of DR5-scFv sEVs with DR5 monoclonal antibody, tigatuzumab, which has the same variable fragment heavy chain (V_H) and variable fragment light chain (V_L) sequences as the scFvs used in the DR5-scFv. A375 cells were treated

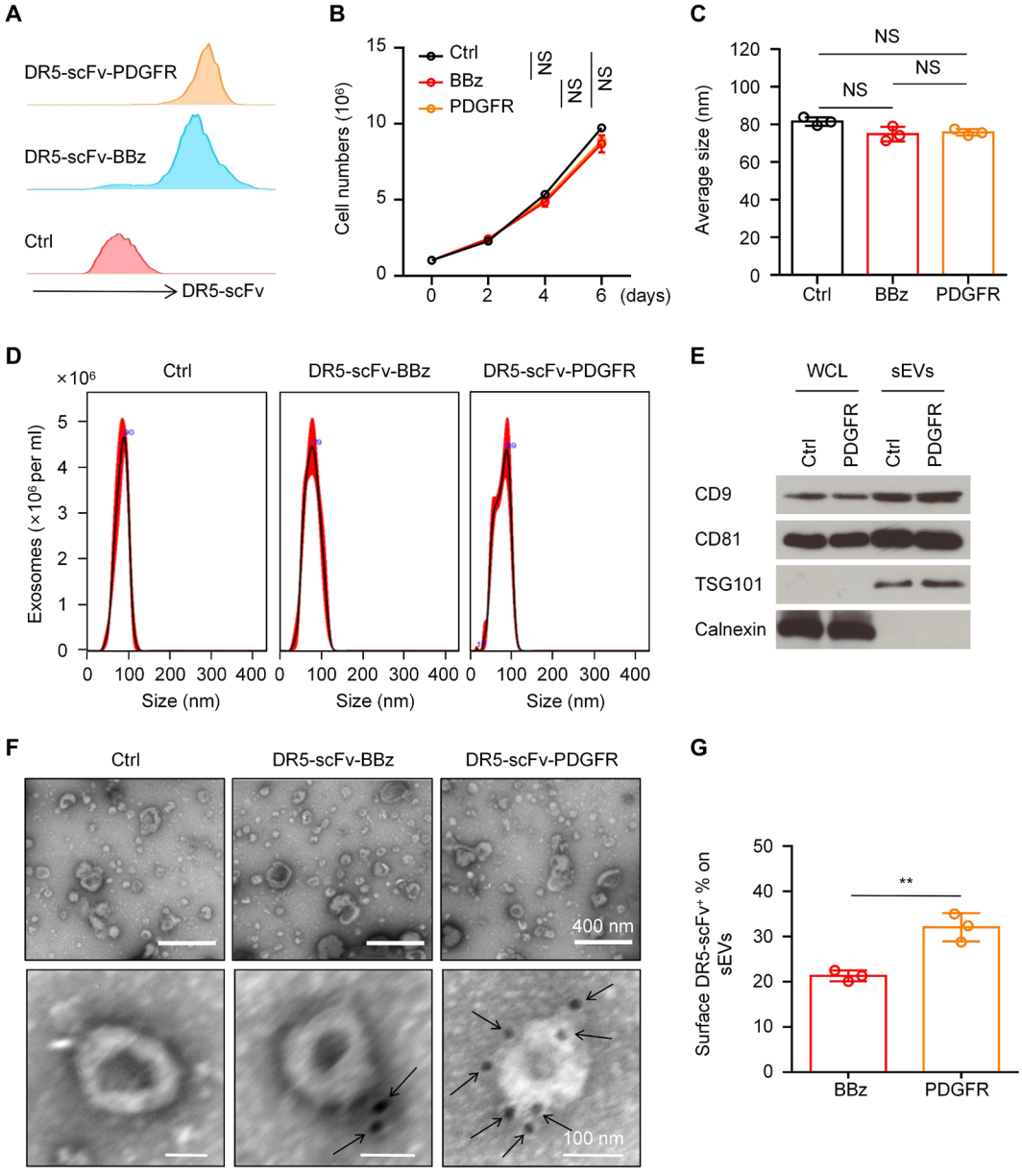

Fig. 2. PDGFR-TM increases the surface expression of DR5-scFvs in sEVs. (**A**) DR5-scFv expression in NK92 cells. NK92 cells were transfected with DR5–4-1BBz or DR5-PDGFR lentiviral vectors. DR5-scFv–positive cells were sorted and cultured. The expression of DR5-scFv in NK92 cells was analyzed using flow cytometry. (**B**) NK92 cell proliferation was not affected by transfection with different vectors. The cell numbers of the control, DR5-BBz-NK92, and DR5-PDGFR-NK92 cells were counted at the indicated time points. Data are presented as means ± SD ($n = 4$). (**C** and **D**) Nanoparticle tracking analysis of sEVs using NanoSight NS300. Representative images and bar charts of the size distribution of sEVs derived from control, DR5–4-1BBz–NK92, or DR5-PDGFR-NK92 cells. (**E**) Immunoblots for sEV markers CD9, CD81, TSG101, and endoplasmic reticulum marker calnexin in NK92 cells whole cell lysate (WCL) and sEVs from NK92 cells. (**F**) Transmission electron microscopy of engineered sEVs. sEVs were labeled with gold-conjugated antibodies against DR5-scFvs. Bars in the upper panels indicate 400 nm, and bars in the lower panels indicate 100 nm. (**G**) On-bead flow cytometry analysis of different types of NK92-derived sEVs. The bar charts show the percentage of DR5-scFv–positive sEVs among different groups. Data are presented as means ± SD ($n = 3$). $^{**}P < 0.01$.

with different amounts of tigatuzumab (1, 2.5, 5, and 10 ng). Using the Avogadro constant and molecular weight of tigatuzumab, we calculated the number of DR5-scFv sEVs needed to have the same number of scFv molecules used in the experiments. The number of sEVs was determined by NTA. DR5-scFv sEVs produced significantly higher cytotoxicity in melanoma cells (Fig. 4, A and B) and liver cancer cells (Fig. 4, C and D) than tigatuzumab in vitro. Furthermore, we performed an in vivo study to compare the effects of DR5-scFv sEVs with DR5 antibodies. Tumor-bearing mice were treated with DR5-scFv EVs (100 μg), low-dose DR5 antibodies (5 ng, similar to the calculated DR5-scFvs in the DR5-scFv EVs), high-dose DR5 antibodies (4.6 μg, 920 times more than the calculated DR5-scFvs in the DR5-scFv EVs), or vehicles. DR5-scFv sEVs showed significantly greater effectiveness in inhibiting melanoma growth compared to high-dose

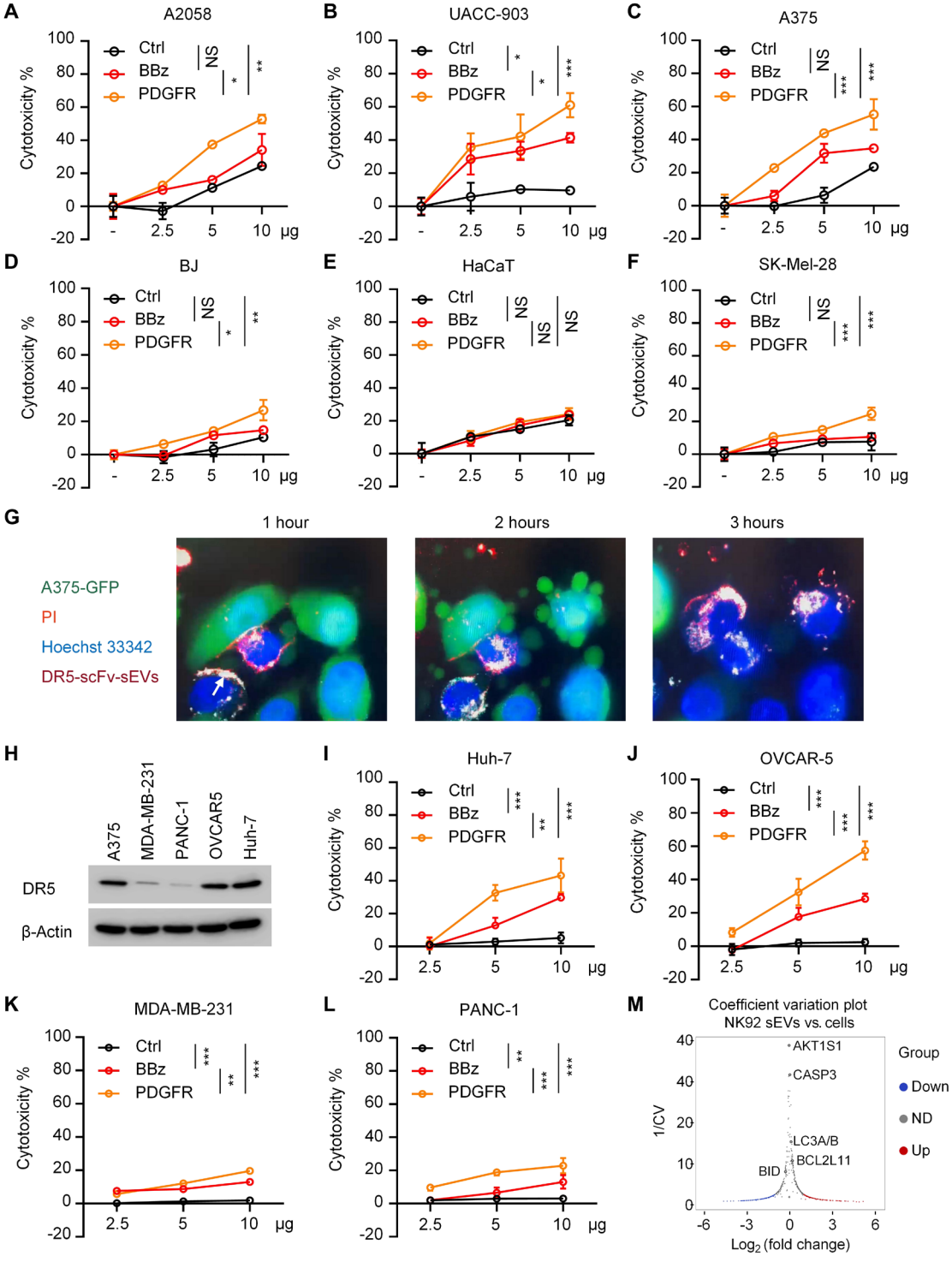

Fig. 3. DR5-scFv sEVs exhibit cytotoxicity to tumor cells in a dose- and DR5 expression–dependent manner. (**A** to **F**) Luciferase-killing assay of DR5-scFv sEVs in different cells. A2058 (A), UACC-903 (B), A375-WT (human melanoma cell lines) (C), BJ (human fibroblast cell line) (D), HaCaT (human keratinocyte cell line) (E), and SK-Mel-28 (human melanoma cell lines) (F) were treated with vehicle, 2.5, 5, or 10 μg of EVs derived from control, DR5-BBz, and DR5-PDGFR-NK92 cells. $^{*}P < 0.05$, $^{**}P < 0.01$, $^{***}P < 0.001$. (**G**) Representative images of A375-GFP cells treated with DR5-scFv sEVs. A375-GFP cells (green) were treated with DR5-scFv sEVs (deep red) for 3 hours. These cells were stained with propidium iodide (red) and Hoechst 33342 (blue). Images were taken at the indicated time points. (**H**) DR5 expression in different epithelial cancer cell lines. Proteins were extracted from different cells and subjected to immunoblot analysis using antibodies against DR5. β-Actin was used as a control. Representative images from three experiments. (**I** to **L**) Luciferase-killing assay of DR5-scFv sEVs in different cancer cells. Huh-7 (human liver cancer cells) (I), OVCAR-5 (human ovarian cancer cell) (J), MDA-MB-231 (human breast cancer cell) (K), and PANC-1 (human pancreatic cancer cell line) (L) were treated with vehicle, 2.5, 5, or 10 μg of sEVs derived from control, DR5–4-1BBz, and DR5-PDGFR-NK92 cells and were subjected to luciferase assays. $^{*}P < 0.05$, $^{**}P < 0.01$, $^{***}P < 0.001$. (**M**) Coefficient variation plot of proteins in NK92 cells and NK92-sEVs. RPPA was performed using 491 antibodies. The *y* axis was the reciprocal of coefficient variation.

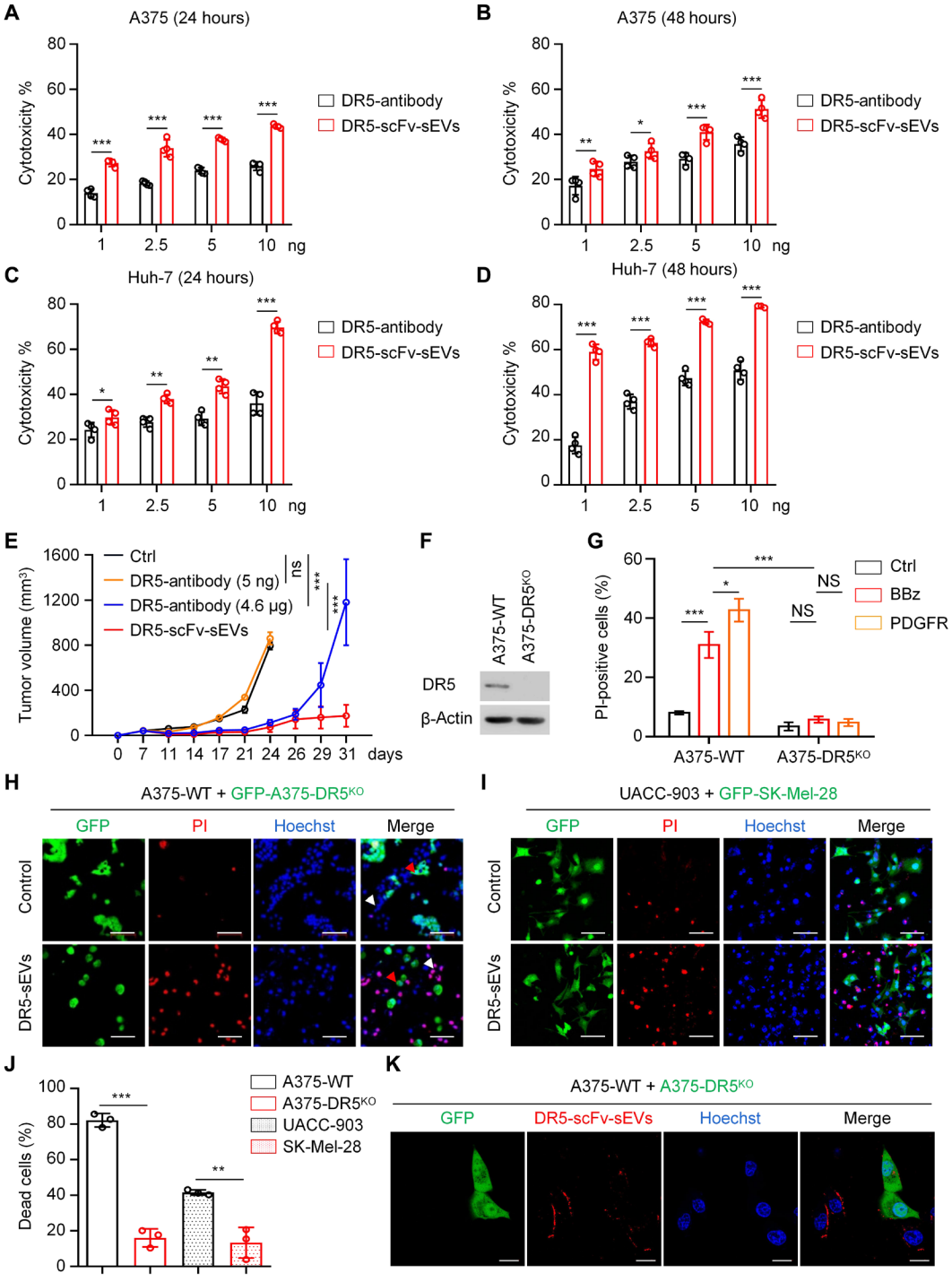

Fig. 4. DR5-scFv sEVs show specificity to DR5^{high} melanoma cells. (**A** to **D**) Luciferase-killing assay using tigatuzumab and DR5-scFv sEVs in A375 and Huh-7 cells. A375 (A and B) and Huh-7 (C and D) cells were treated with equivalent DR5 antibody molecules or DR5-scFvs in the sEVs. (**E**) Low-dose DR5 antibody (5 ng), high-dose DR5 antibody (4.6 μg), or DR5-scFv sEVs (100 μg per mouse) were injected through the tail vein into the nude mice ($n = 5$). Treatment was given twice a week. Tumor volume was measured at the indicated time points. (**F**) Immunoblot analysis of proteins from A375-DR5^{WT} and A375-DR5^{KO} cells. DR5 in A375 was knocked out using CRISPR/Cas9. (**G**) DR5-scFv sEVs induce apoptosis in melanoma cells. A375-DR5^{WT} and A375-DR5^{KO} cells were treated with indicated sEVs for 24 hours and stained with PI. Bar charts show the percentage of PI-positive melanoma cells ($n = 3$). (**H** to **J**) DR5-scFv sEVs induce more apoptosis in DR5^{high} cells than in DR5^{low} cells. A375-DR5^{WT} (without GFP tag) and A375-DR5^{KO} (with GFP tag) cells (H), or UACC-903 (without GFP tag) and SK-Mel-28 (with GFP tag) cells (I) were mixed and incubated with 10 μg of DR5-scFv sEVs or control sEVs for 24 hours. PI (red) and Hoechst 33342 (blue) staining were performed (scale bar = 50 μm). (J) Bar chart of the percentage of dead cells ($n = 3$). (**K**) DR5-scFv sEVs preferentially bind to DR5 wild-type cells. DR5-scFv sEVs were labeled with a Deep Red dye (red). A375-DR5^{WT} (without GFP tag) and A375-DR5^{KO} (with GFP tag) cells were incubated with pre-dyed DR5-scFv sEVs for 2 hours. Representative images of the uptake of DR5-scFv sEVs by A375 cells were taken. Scale bar, 5 μm. *$P < 0.05$, **$P < 0.01$, ***$P < 0.001$.

DR5 antibodies (4.6 μg). In contrast, low-dose DR5 antibodies (5 ng) did not effectively control tumor growth (Fig. 4E). In addition, the high-dose DR5 antibodies induced cachexia in two of the five treated mice, but none of the mice treated with DR5-scFv EVs developed apparent adverse reactions. These findings suggest that DR5-scFv sEVs offer advantages over DR5 monoclonal antibodies in controlling tumor growth.

Targeting specificity of DR5-scFv sEVs

To study the specificity of DR5-scFv sEV-induced targeted cell death, we knocked out DR5 in A375 cells (A375-DR5^{KO}) using CRISPR/Cas9 (Fig. 4F). After DR5 knockout, the cytotoxic effect of DR5-scFv sEVs on A375-DR5^{KO} cells was significantly diminished. sEVs from control, DR5-BBz-NK92, and DR5-PDGFR-NK92 cells showed similar cytotoxic effects to A375-DR5^{KO} cells (Fig. 4G and fig. S7). To further confirm the specificity of DR5-scFv sEVs, we cocultured GFP-tagged A375-DR5^{KO} cells with A375-DR5^{WT} cells (without GFP tag) on the same plate. Dead cells were noticeably increased after treatment with DR5-scFv sEVs, mostly in unlabeled A375-DR5^{WT} cells. GFP-tagged DR5^{KO} cells were only slightly affected (Fig. 4H). Approximately 80% of DR5^{WT} cells were killed after treatment, whereas less than 20% of DR5^{KO} cells were dead (Fig. 4J). Similar results were observed for cocultured DR5^{high}-UACC-903 (without GFP tag) with DR5^{low}-SK-Mel-28 (with GFP tag) cells (Fig. 4, I and J), suggesting that DR5-scFv sEVs induce tumor cell death in a DR5 expression level–dependent manner.

To further investigate how DR5-scFv sEVs induce DR5^{+} cell apoptosis, we examined whether DR5-scFv sEVs preferentially bind to DR5^{+} cells. DR5-scFv sEVs were labeled with a Deep Red dye. The labeled sEVs were added to a mixed culture of A375-DR5^{WT} (without the GFP tag) and GFP-tagged A375-DR5^{KO} cells for 2 hours. Fluorescent microscopy showed that labeled DR5-scFv sEVs preferentially bound to A375-DR5^{WT} cells compared to A375-DR5^{KO} cells (Fig. 4K), supporting that DR5-scFv sEVs preferentially bind to DR5^{+} tumor cells.

Freezing/thaw processes have minimal effects on DR5-scFv sEVs

The tumor-killing effect of DR5-scFv sEVs could be enhanced by extending the treatment time or increasing the concentration of sEVs (fig. S8, A and B). To develop off-the-shelf therapies, it is essential to freeze and thaw the products. We compared the cytotoxicity of fresh and frozen/thawed DR5-scFv sEVs in A375 cells. We found no significant difference after a freeze-thaw cycle (fig. S8C), indicating that the sEVs were stable during the freeze-thaw cycle.

DR5-scFv sEVs efficiently penetrate melanoma spheroids

A critical barrier in cellular therapy for solid tumors is the tumor-homing barrier, as the immunosuppressive TME prevents T cells from migrating into the tumor (*1*). We previously showed that bicellular three-dimensional (3D) melanoma spheroids composed of melanoma cells and CAFs mimic patient-derived melanoma organoids and significantly decrease T cell infiltration compared to unicellular 3D spheroids composed of melanoma cells (*30*). Bicellular 3D melanoma spheroids were formed by mixing GFP-tagged A375-DR5^{WT} or GFP-tagged A375-DR5^{KO} with BJ cells at a ratio of 1:2 in a 1.5% agarose precoated 96-well plate for 24 hours. The spheroids were treated with 10 μg of sEVs derived from control, DR5-BBz-NK92, or DR5-PDGFR-NK92 cells for 24 hours. DR5-scFv sEVs induced cell death in A375-DR5^{WT} spheroids, as dead GPF^{+} tumor cells lost green fluorescence and gained PI staining. DR5-scFv sEVs were less effective in killing A375-DR5^{KO} spheroids (fig. S8D).

Effect of DR5-scFv sEVs on DR5^{+} cancers in vivo

To investigate the effect of DR5-scFv sEVs in vivo, we developed a model with DR5^{WT} and DR5^{KO} melanoma xenografts in NOD scid gamma (NSG) mice. A375-DR5^{WT}-GFP-ffLUC cells were seeded in the right flank of mice, and A375-DR5^{KO}-GFP-ffLUC cells were seeded in the left flank. DR5^{KO} melanomas grew faster than DR5^{WT} melanomas. Using this model, we first examined the homing of DR5-scFv sEVs. When the tumors were palpable 10 days after implantation, we injected the Deep Red–labeled DR5-scFv sEVs or labeled control sEVs into the tumor-bearing mice through the tail veins (Fig. 5A). In vivo fluorescence imaging studies revealed that 1 hour after injection, DR5-scFv sEVs were already present in the A375-DR5^{WT} tumors. In contrast, much fewer labeled sEVs were present in the contralateral A375-DR5^{KO} tumors, although these tumors were larger in size. Twenty-four hours later, labeled DR5-scFv sEVs were still observed in A375-DR5^{WT} tumors. In contrast, control sEVs showed no specific accumulation on either side of the mice (Fig. 5, B and C). These data indicate that DR5-scFv sEVs preferentially migrate to DR5^{+} tumor cells in vivo and that the TME does not prevent the entrance of sEVs.

We next examined the effect of DR5-scFv sEVs on tumor growth. A375-DR5^{WT} cells were implanted into nude mice. After the tumors became palpable, PBS, control sEVs (from NK92 cells), or DR5-scFv sEVs (from DR5-PDGFR-NK92 cells) were injected intratumorally into the mice every 3 days for six treatments (fig. S9A). Control sEVs from NK92 produced significantly more tumor growth inhibition than the PBS control. DR5-scFv sEVs showed significantly more tumor growth inhibition than control sEVs (Fig. 5D and fig. S9B). We then tested the efficacy of the systemic delivery of DR5-scFv sEVs on melanoma growth. When tumors became palpable, sEVs were injected via the tail vein into tumor-bearing mice every 3 days (fig. S9C). Similar to the results of intratumor treatment, systemic DR5-scFv sEVs also significantly inhibited melanoma growth (Fig. 5E and fig. S9D) and prolonged the survival of the treated mice (Fig. 5F). We examined the expression of cleaved CASP3 in sEV-treated tumors. The results showed that the residual melanoma cells expressed higher levels of cleaved CASP3 after treatment with DR5-scFv EVs (Fig. 5G). Weight loss was not observed during the treatment (fig. S9, E and F), nor was lethargy or other signs of adverse reactions in mice, suggesting the therapy was safe. In addition, we performed an in vivo dose escalation study to further examine the safety of DR5-scFv sEVs. Mice received multiple doses of 500, 1000, and 1500 μg of sEVs, and none of the mice developed signs of toxicity (fig. S10).

The effects of DR5-scFv sEVs on other tumors were also examined. Mouse xenograft models of WM4625.2brm (melanoma), MDA-MB-231brm (breast cancer), and Huh-7 (liver cancer) were established. When the tumors became palpable, PBS or DR5-scFv sEVs were injected through the tail vein at the indicated time points (fig. S11, A and B). DR5-scFv sEVs significantly inhibited the growth of these tumors (Fig. 5, H to J, and fig. S11, C to E) and prolonged survival of the treated mice (Fig. 5, K to M). There was little impact on the body weight of mice (fig. S11, F to H).

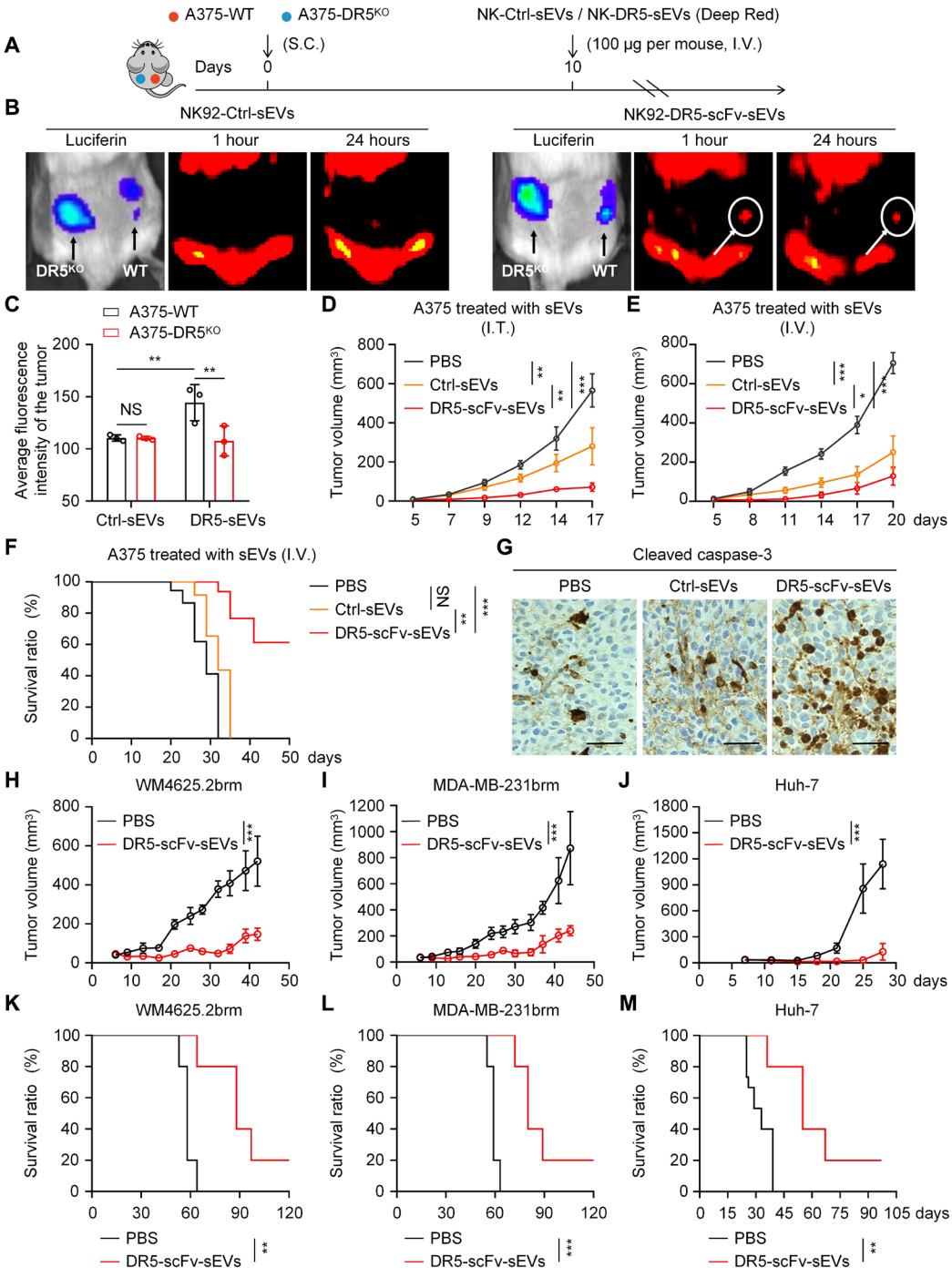

Fig. 5. DR5-scFv sEVs migrate to DR5^{+} melanoma and inhibit tumor growth in vivo. (**A**) Melanoma xenograft mouse model was established by subcutaneous (S.C.) injection of A375-DR5^{WT} cells into the right flank and A375-DR5^{KO} cells into the left flank of NSG mice. Pre-dyed control sEVs or DR5-scFv sEVs (100 μg per mouse, red) were injected into the mice at the indicated times through the tail vein [intravenously (I.V.)]. (**B**) Representative images of tumors and labeled sEVs at the indicated time points. Tumors were imaged using luciferin. (**C**) Bar chart of the average fluorescence intensity in the different groups ($n = 3$ per group). $^{**}P < 0.01$. (**D** to **G**) DR5-scFv sEVs suppressed melanoma tumor growth in vivo. DR5-scFv sEVs (100 μg per mouse) or equivalent volume of PBS was injected intratumorally (D) through the tail vein [(E) to (G)] or into the mice ($n = 5$ per group). [(D) and (E)] Tumor volume was measured at the indicated time points. (F) Kaplan-Meier survival curve of mice in the three groups. $^{*}P < 0.05$, $^{**}P < 0.01$, $^{***}P < 0.001$. (G) DR5-scFv sEVs induced apoptosis in melanoma cells. Immunohistochemical staining of mouse tumor tissues for cleaved caspase-3 was performed. Scale bar, 100 μm. (**H** to **M**) DR5-scFv sEVs inhibit the growth of multiple different types of tumors in vivo. Xenograft mouse models were established by subcutaneous injection of WM4625.2brm, MDA-MB-231brm, or Huh-7 cells into the right flank of the nude mice. DR5-scFv sEVs (100 μg per mouse) or an equivalent volume of PBS was injected through the tail vein (intravenously) into the mice ($n = 5$ per group). Tumor volumes were measured at the indicated times. $^{*}P < 0.05$, $^{**}P < 0.01$, $^{***}P < 0.001$. [(K) to (M)] Kaplan-Meier survival curve of tumor-bearing mice in different groups. $^{*}P < 0.05$, $^{**}P < 0.01$, $^{***}P < 0.001$.

DR5-scFv sEVs are cytotoxic to MDSCs and CAFs

The immunosuppressive TME hinders cellular therapy by preventing T cell entry and inducing T cell exhaustion. It is well known that DR5 is highly expressed in MDSCs (*31*). Our DR5 immunohistochemical staining of melanoma tissues showed that DR5 was highly expressed in melanoma cells (Fig. 6A), as well as in some of the immune cells (Fig. 6B) and spindle-shaped fibroblasts (Fig. 6C). To study the effects of DR5-scFv EVs on these cells, we first induced MDSCs from human PBMCs using granulocyte-macrophage colony-stimulating factor (GM-CSF) and interleukin-6 (IL-6) and then treated these MDSCs with DR5-scFv sEVs for 24 hours. FACS analysis showed that induced MDSCs were significantly inhibited by DR5–4-1BBz sEVs and DR5-PDGFR sEVs (Fig. 6D and fig. S12). These results were further confirmed by the cytotoxicity assays (Fig. 6E). As melanoma tissue is rich in MDSCs (*32*), we treated fresh patient-derived melanoma tissue slices (*33*) with DR5-scFv sEVs. The percentage of MDSCs in fresh melanoma tissues was significantly reduced after DR5-scFv sEV treatment (Fig. 6, F and G, and fig. S13). The sEVs from DR5-PDGFR-NK92 showed the highest therapeutic efficiency.

To study the effect of DR5-scFv sEVs on CAFs, we induced CCD19-Lu, a human fibroblast cell line, into CAFs by coculture with the supernatant from melanoma cells. DR5 expression was higher in CAFs than normal fibroblasts (Fig. 6H). The cytotoxicity assay demonstrated that DR5-scFv sEVs effectively killed CAFs in a dose-dependent manner compared to the control cells (Fig. 6, I and J). Our data suggest that DR5-scFv sEVs are cytotoxic to MDSCs and CAFs.

DR5-scFv sEVs reprogram the TME in melanoma

To determine the tumor-killing efficiency of DR5-scFv sEVs in fresh melanoma tissues, we treated patient-derived organotypic melanoma slices with sEVs for 24 hours and measured cell apoptosis using annexin V and 7-aminoactinomycin D (7-AAD) apoptosis assays. The number of apoptotic cells in fresh melanoma tissues derived from eight patients significantly increased after treatment with DR5-scFv sEVs (Fig. 7, A and E). The percentage of $CD8^+$ T cells significantly increased in melanoma slices after DR5-scFv sEV treatment (Fig. 7, B and F). The levels of granzyme B (Fig. 7, C and G) and Ki-67 (Fig. 7, D and H) were significantly elevated in DR5-scFv sEV–treated samples, indicating that DR5-scFv sEVs can activate $CD8^+$ T cells in the TME (fig. S14). In addition, we incubated PBMCs from healthy donors with vehicle, NK92-Ctrl sEVs, or NK92-DR5 sEVs for 48 hours. The results showed that sEVs derived from NK92 cells could stimulate the expression of granzyme B (fig. S15).

DISCUSSION

EVs are approximately 1 million times smaller than T cells in volume. Unlike CAR-T cells, sEVs can readily penetrate the immune barrier in the TME (*27*, *28*), travel to immune-privileged sites (*34*), and enter solid tumors (*35*). Our study showed that DR5 CAR-T cells effectively controlled A375 melanoma growth when injected intratumorally but not systemically in nude mice. On the contrary, DR5-scFv sEVs effectively control tumor growth in multiple solid tumor models after systemic delivery. DR5-scFv sEVs retained tumor-targeting ability similar to CAR-T cells as they migrated to $DR5^+$ cells in vitro and in vivo. DR5-scFv sEVs were more cytotoxic than DR5 antibodies. Moreover, DR5-scFv sEVs inhibited the proliferation of MDSCs and CAFs and stimulated $CD8^+$ T cells in the TME. These data suggest that DR5-scFv sEVs have advantages over DR5 CAR-T cells in solid tumor treatment. These engineered sEVs may represent promising off-the-shelf immunotherapy since DR5-scFv sEVs can be mass-produced using the engineered NK92 cell lines.

EV-based therapies can potentially address some challenges that CAR-T cell therapies face in solid tumors, such as antigen specificity and undesirable life-threatening adverse effects. Tumor-associated antigens in solid tumors are not as specific as in hematopoietic malignancy, which may result in severe adverse effects from CAR-T therapies, such as cytokine release syndrome (CRS) (*36*–*38*). CAR-T cell–derived sEVs did not induce changes in serum cytokine levels and body weight in mice, while their parental CAR-T cells killed all the treated mice in 48 hours with CRS-like cytokine changes in the circulation (*39*, *40*). Treatment of patients with advanced non–small cell lung cancer using dendritic-derived sEVs showed no severe toxicity or organ damage (*41*). Unlike T cells, sEVs do not expand in patients. As such, the potential adverse reactions to sEVs are likely transient and manageable (*42*). In addition, CAR-T cell therapy requires lymphodepletion, which has severe side effects (*43*), while lymphodepletion is not needed for EV-based therapies. Thus, EV-based therapies are inherently safer than CAR-T therapies.

DR5-scFv sEVs are more cytotoxic to melanoma cells than antibodies with the same scFv because they can combine the advantages of both scFv fragments and sEVs. sEVs from NK92 cells carry various bioactive molecules, such as perforin, granzymes, Fas ligand (FasL), and TRAIL (*8*). When NK92 cell–derived sEVs interact with tumor cells, the cytotoxic molecules may be transferred to the tumor cells, triggering programmed cell death (*44*). The lipid bilayer in the sEVs can protect surface scFvs from degradation in circulation (*45*). Displaying scFv on the surface of sEVs can improve their specificity and targeting capabilities. sEVs can carry multiple copies of the scFvs, increasing the avidity for the target antigen and potentially improving the binding affinity (*46*).

DR5 agonistic scFvs are different from other reported scFvs used in CAR vectors in the literature because they not only provide specificity toward target cells but also directly induce target cell apoptosis upon binding. Our second-generation DR5–4-1BBz CAR delivered fewer DR5-scFvs to the surface of sEVs than the PDGFR-TM version. Fusing target proteins or peptides with transmembrane proteins expressed on the surface of sEVs, such as lysosome-associated membrane protein (LAMP-2B) and PDGFR, has been tested for membrane motif loading (*29*, *47*). The cytotoxic effect of DR5-scFv sEVs on tumor cells was significantly increased with more DR5-scFvs on the surface of sEVs. Surface DR5-scFvs allow these sEVs to selectively target $DR5^+$ cells in vitro and in vivo and enhance their tumor-killing effects. Increasing the surface expression of specific scFvs on sEVs is a practical strategy to improve the functions of engineered sEVs.

DR5 is highly expressed in tumors, MDSCs, and CAFs (*48*, *49*), which are critical immunosuppressive components of the TME. The immunosuppressive TME fails to deter the infiltration of DR5-scFv sEVs when administered systemically. sEVs are less susceptible than CAR-T cells to the immunosuppressive effects in the TME (*50*). Thus, MDSCs and CAFs can be targeted by DR5-scFv sEVs. In addition, sEVs from NK92 cells may also carry cytokines, chemokines, miRNAs, and other signaling molecules that can reprogram the TME and promote an inflammatory response against tumor cells (*51*). Our patient-derived melanoma slice culture demonstrated that these engineered sEVs stimulated $CD8^+$ T cell functions in the TME.

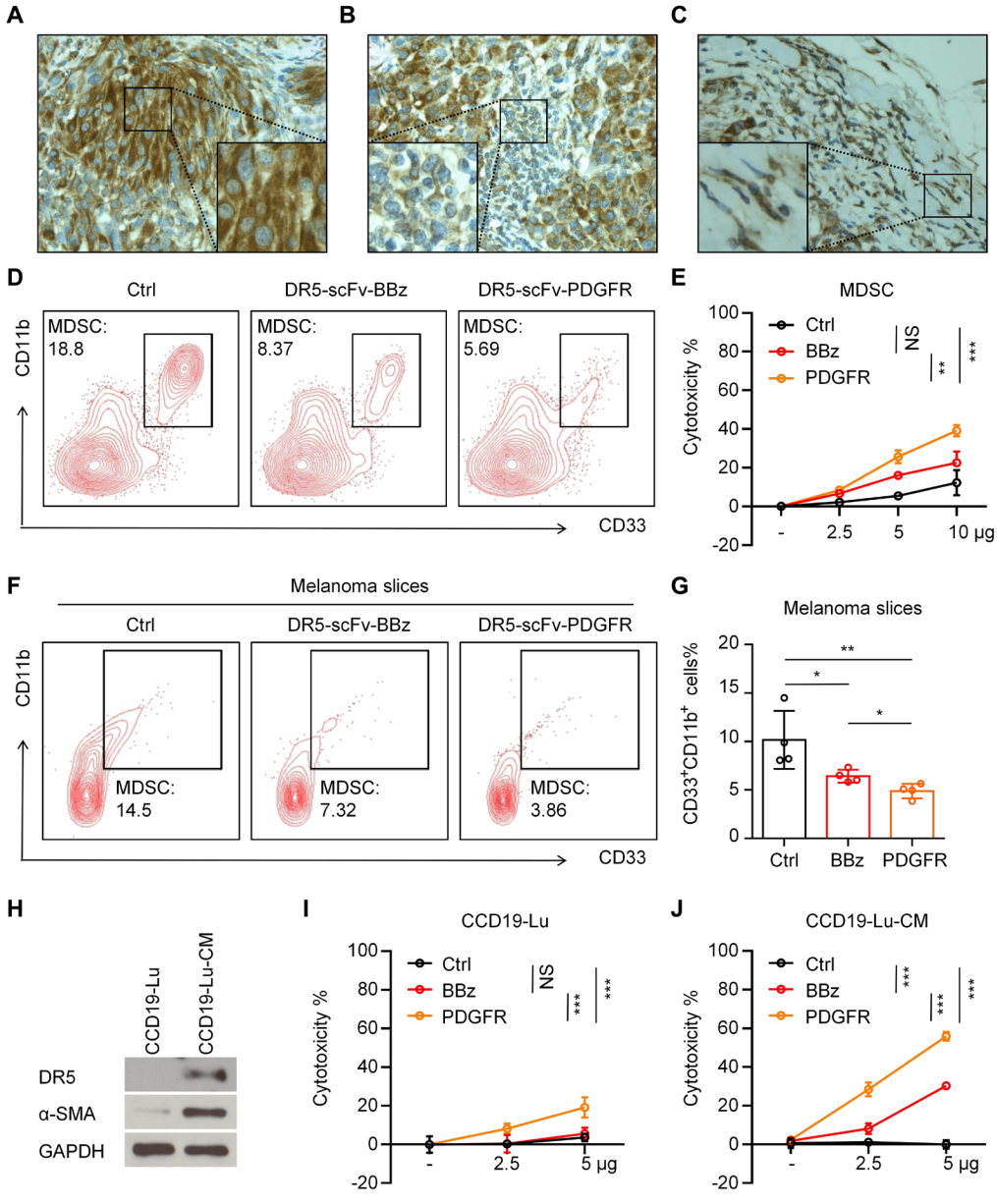

Fig. 6. DR5-scFv sEVs target MDSCs and CAFs in melanoma. (**A** to **C**) DR5 is highly expressed in melanoma cells (A), MDSCs (B), and CAFs (C) in melanoma patient tissues as detected by immunohistochemistry. (**D** and **E**) DR5-scFv sEVs showed cytotoxicity to MDSCs. MDSCs were induced by GM-CSF and IL-6 and treated with indicated sEVs for 24 hours. (D) Flow cytometry plots show the percentage of $CD33^+CD11b^+$ cells among the different groups. (E) Killing assay of indicated sEVs on MDSCs. Data represent means ($n = 3$) ± SD of each group. $^*P < 0.05$, $^{**}P < 0.01$, $^{***}P < 0.001$. (**F** and **G**) DR5-scFv sEVs kill MDSCs in organotypic patient-derived melanoma tissue slices. Tissue slices of organotypic melanoma were obtained and treated with sEVs. Flow cytometry plots of $CD33^+CD11b^+$ MDSC (F) and bar charts of the percentage of $CD33^+CD11b^+$ live cells in different groups (G) are shown. Data represent means ($n = 4$) ± SD of each group. $^*P < 0.05$, $^{**}P < 0.01$, $^{***}P < 0.001$. (**H**) DR5 was highly expressed in CAFs induced by CCD19-Lu cells. Artificially induced CAFs are generated. Proteins were extracted from the cells and subjected to immunoblot analysis using antibodies against DR5. β-Actin was used as a control. (**I** and **J**) CAF killing assay using DR5-scFv sEVs. Control CCD19-Lu cells (I) and induced CAFs (J) were treated with vehicle, 2.5, 5, or 10 μg of sEVs derived from control, DR5-BBz-NK92, and DR5-PDGFR-NK92 cells. Data represent means ($n = 3$) ± SD of each group. $^*P < 0.05$, $^{**}P < 0.01$, $^{***}P < 0.001$.

Primary cells, particularly T cells, are difficult to manipulate because of their low transfection rates (*52*). Immortalized cell lines are recognized as more stable and convenient for preparing sEVs. The NK92 cell line has been U.S. Food and Drug Administration–approved for cancer immunotherapy and has been investigated in clinical trials (*53*). One major limitation for sEVs to reach their full potential is their limited yields from cells, particularly from attached primary cells, which constitutes a major bottleneck for large-scale EV production (*54*). Well-characterized cell lines are recognized as being better than primary cells for EVs' uniformity, batch-to-batch consistency, and stability. Therefore, the NK92 cell–based EV production method can significantly reduce the manufacturing cost and batch-to-batch variation for future regulatory approval. Designer sEVs from NK92 cells can be mass-produced and used as an off-the-shelf therapy.

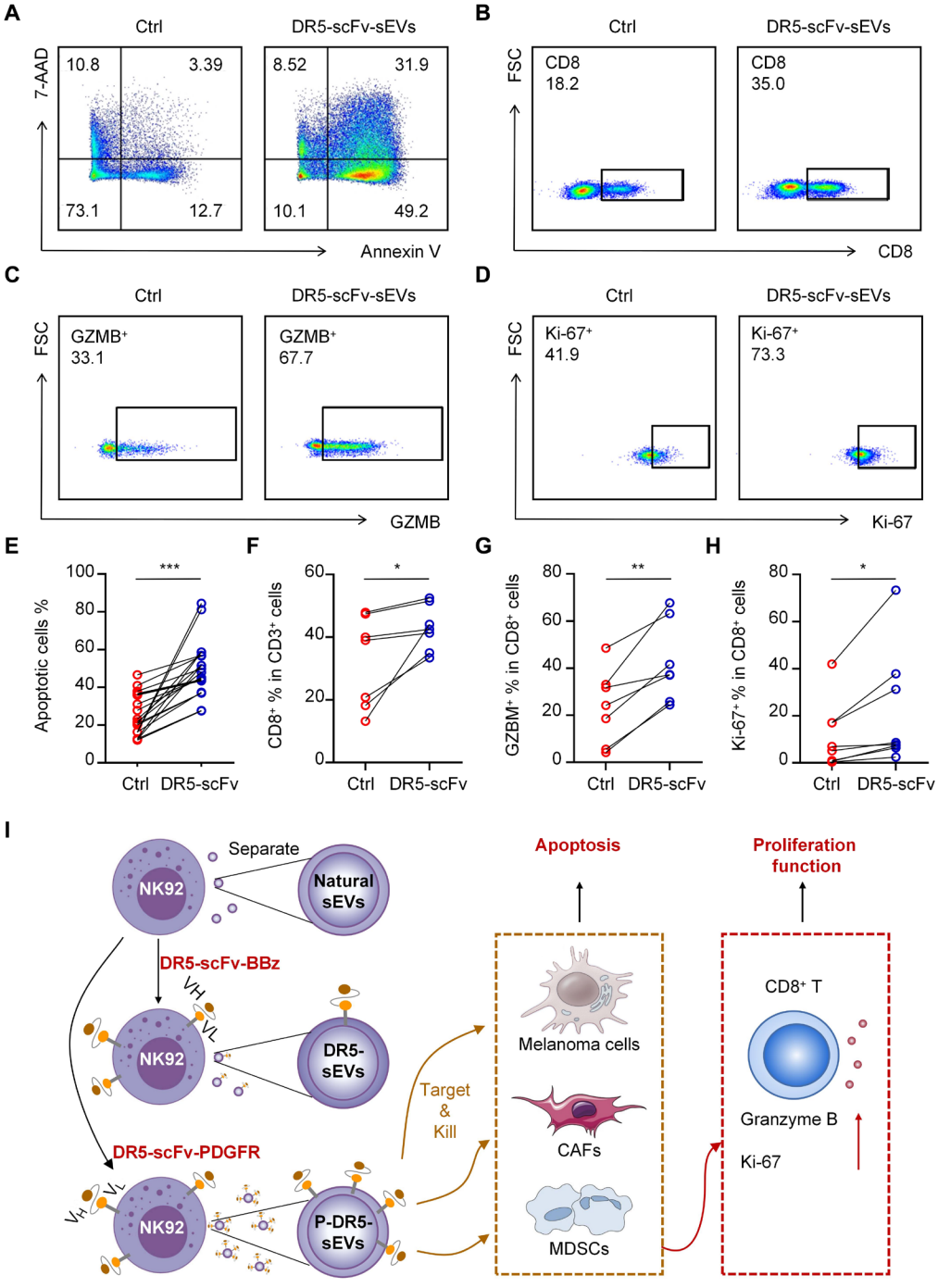

Fig. 7. DR5-scFv sEVs exert cytotoxicity in melanoma tissue slices and enhance the functions of tumor tissue–resident CD8$^+$ T cells. (**A**) DR5-scFv sEVs induce apoptosis in melanoma tissue slices. sEV-treated tumor slices were subjected to annexin V apoptosis assays. Representative flow cytometry plots of apoptotic cells in control or DR5-scFv sEV–treated melanoma slices are shown. (**B** to **D**) DR5-scFv sEVs increase CD8$^+$ T cell function in patient-derived melanoma tissue slices. Representative flow cytometry plots of the percentage of CD8$^+$ T cells among CD3$^+$ cells (B), percentage of granzyme B (C), and Ki-67 (D) among CD8$^+$ T cells. (**E**) Bar chart of apoptotic cells in different melanoma slices derived from eight patients. *$P < 0.05$, **$P < 0.01$, ***$P < 0.001$. (**F** to **H**) Bar chart of the percentage of CD8$^+$ T cells in CD3$^+$ cells (F), percentage of granzyme B (G), and Ki-67 (H) in CD8$^+$ T cells in different groups. *$P < 0.05$, **$P < 0.01$. (**I**) Schematic diagram of DR5-scFv sEVs reprograming the TME may be developed as a novel cancer therapy.

The purification and clinical application of EVs still face significant hurdles. A major challenge is the lack of standardized isolation and purification protocols, leading to variability in EV preparations and hampering reproducibility across studies (*55*). Current isolation methods like ultracentrifugation often result in low yields and co-isolation of non-EV contaminants, compromising purity (*56*). The heterogeneity of EV populations further complicates the quality control processes essential for clinical-grade production (*57*). Regulatory hurdles, including the lack of clear guidelines for EV-based therapeutics and difficulties in standardizing good manufacturing practice (GMP)–compliant processes, further impede clinical translation. Overcoming these challenges in EV production, characterization, and engineering is crucial for realizing the full potential of EVs in clinical applications. Despite these challenges, 66 EV-based interventional clinical trials are ongoing (*58*), supporting the validity of EV-based therapies.

Together, we have developed engineered sEVs expressing a high level of DR5-scFvs. These armed sEVs specifically target $DR5^+$ tumor cells, MDSCs, and CAFs. Inhibition of these cells alleviates the immunosuppressive TME, allowing other immune cells, such as $CD8^+$ T cells, to function properly (Fig. 7I). Our results suggest that engineered DR5-scFv sEVs represent a promising strategy for cancer immunotherapy. It is possible to arm the sEVs with different scFvs to target various cancers, making it a versatile off-the-shelf platform technology that can be adapted to treat solid cancers.

METHODS

Cell lines and cell culture

NK92 cell line (American Type Culture Collection, MD, USA) was cultured in minimum essential medium α medium with 10% fetal bovine serum (FBS), 10% horse serum, 0.2 mM myo-inositol, 0.1 mM 2-mercaptoethanol (2-Me), 0.02 mM folic acid, recombinant human IL-2 (200 U/ml), and 1% penicillin-streptomycin at 37°C and 5% CO_2. The human fibroblast cell lines BJ and CCD19-Lu were maintained in Eagle's minimum essential medium with 10% FBS and 1% penicillin-streptomycin at 37°C and 5% CO_2. The human keratinocyte cell line HaCaT and melanoma cell lines including A375, UACC-903, A2058, SK-Mel-28, and human embryonic kidney (HEK) 293T were maintained in Dulbecco's modified Eagle's medium (DMEM) at 37°C and 5% CO_2. The reagents used are listed in table S1.

Generation and expansion of MDSCs in vitro

MDSCs were expanded from PBMCs and cultured in complete RPMI 1640 containing GM-CSF (100 ng/ml) and IL-6 (100 ng/ml) at a density of 5×10^6 cells/ml for 7 days.

Induction of CAFs in vitro

A375 melanoma cells (5×10^6) were seeded in a 10-cm cell culture dish and replaced with fresh culture medium when the cells had reached the desired confluence, and the culture was continued for 48 hours. The medium was then collected and filtered through a 0.22-μm polyethersulfone (PES) filter to remove cells and cellular debris. CCD19-Lu cells were cultured in conditioned medium and fresh culture medium (1:1) for 48 hours to induce the CAF phenotype.

Vector construction

DR5 antibody sequences were obtained from the IMGT (mAB-DB ID 183, 224, 234, and 348). The DNA fragments of the variable domains of V_H and V_L were fused and linked with a -$(G_4S)_3$- linker and flanked by a human-CD8 leader and a human-IgG4 (immunoglobulin G4) hinge. The scFv sequence was synthesized by Integrated DNA Technologies (IDT; NJ, USA). These cDNAs were then cloned into an engineered pTRPE CAR encoding lentiviral backbone. PDGFRTM was synthesized by IDT and cloned into DR5–4-1BBz–CAR to replace CD8 TM, 4-1BB, and CD3ζ domains.

Lentivirus packaging

Lentiviral vector packaging was carried out using HEK293T cells. A transfection mixture was prepared by combining 10 μg of the lentiviral vector plasmid, 7.5 μg of pMDLg/pRRE, 2.5 μg of pRSV-Rev, and 2.5 μg of pCMV-VSVG in 500 μl of serum-free RPMI 1640. Premixed Lipofectamine 2000 was added to the mixture and incubated for 20 min at room temperature. The transfection mix was added to the cells and incubated for 6 to 8 hours at 37°C in a 5% CO_2 incubator. Half volume of full RPMI 1640 containing 10% FBS was added after transfection. After 24 and 48 hours, lentivirus-containing supernatant was collected, filtered, and concentrated overnight by ultracentrifugation at 12,000 rpm. The final lentivirus particles were aliquoted and can be stored at −80°C until needed.

T cell expansion and CAR-T cell transduction

Isolated human PBMCs were cultured with CD3/28 Dynabeads at a 1:1 cell-to-bead ratio in RPMI 1640 supplemented with 10% FBS (HyClone; GE Healthcare, Utah, USA), penicillin-streptomycin (100 U/ml), 2 mM L-glutamine, 1:1000 2-Me (Gibco; Thermo Fisher Scientific, Massachusetts, USA), and recombinant human IL-2 (100 U/ml) (PeproTech, New Jersey, USA); new medium was added and supplemented every other day. The cells were incubated at 37°C with 5% CO_2 for 24 hours before transduction with CAR lentiviral vectors at multiplicity of infection (MOI) = 1. The medium and IL-2 were replenished every 24 to 48 hours as required. After 7 days, the activated T cells were harvested for further purification, analysis, and downstream applications.

Preparation of sEVs

Cells were cultured in medium as described previously, but FBS and horse serum were EV-depleted by overnight centrifugation at 100,000*g*. Supernatants were collected from 48-hour cell cultures, and sEVs were purified following the standard differential centrifugation protocol (*59*). Briefly, the supernatants were centrifuged at 2000*g* for 20 min to remove cell debris and dead cells, followed by centrifugation at 16,500*g* for 45 min to remove the microvesicles. The supernatants were then centrifuged at 100,000*g* for 2 hours at 4°C. The pelleted sEVs were suspended in PBS and collected. For some functional studies, sEVs were purified using ExoQuick-TC ULTRA (SBI, CA, USA), following the manufacturer's instructions. In brief, 1 volume of ExoQuick-TC ULTRA was added to 5 volumes of sample, mixed well, and incubated overnight at 4°C. The mixture was centrifuged at 3000*g* for 10 min, and the pellet was resuspended. Then, resuspended sEVs were added to prewashed ExoQuick-TC ULTRA columns. Place the column in a 1.5-ml tube and centrifuge at 3000*g*. Discard the column, and the remaining liquid in the 1.5-ml tube is the sEVs. sEV yield per million cells was 1.02 to 1.8 μg.

For freeze/thaw processes, we packaged sEVs into 1 mg/tube, froze, and stored them in a −80°C freezer for subsequent experiments. The frozen time of sEVs ranges from 1 week to 6 months. The frozen sEVs were thawed only once; we did not re-freeze them. For the in vitro and in vivo experiment, we routinely use freeze/thaw sEVs.

3D spheroid formation

The 96-well plate was precoated with 50 μl of 1.5% agarose (50010, Lonza, ME, USA). A375 cells (1×10^4) and BJ cells (2×10^4) were mixed, seeded per well, and allowed to form spheroids for 48 hours.

Organotypic melanoma tissue slice culture

The fresh tumor tissues were kept on ice and sliced using a vibrating microtome for 1 hour. Tissue preparation was performed according to a previously described protocol (*27*). Briefly, the tissues were collected and embedded in 2% agarose for slicing. After the agarose solidified, it was fixed to a specimen disc and sliced using Compresstome VF-310-0Z at a thickness of 500 μm. The tissue slices were placed into a Millicell insert (PIHP01250, Millipore, MO, USA) in a 24-well plate and cultured in RPMI 1640 with 10% FBS, 2 mM L-glutamine (A2916801, Gibco), 10 mM Hepes (15630080, Gibco), 1 mM sodium pyruvate (11360070, Gibco), 5.5 μM 2-Me, 1% penicillin-streptomycin, and IL-2 (200 IU/ml).

Luciferase-killing assay

Cells subjected to the luciferase-killing assay were infected with pCCLc-MNDU3-Luciferase-PGK-EGFP-WPRE (89608, Addgene, MA, USA) and sorted by flow cytometry. According to the manufacturer's instructions, the cytotoxicity assay was performed using the Luciferase Assay System (E1501, Promega, WI, USA). Briefly, target cells were seeded at 4×10^4 cells per well in 96-well plates, while sEVs or effect cells were seeded at the corresponding doses or ratios simultaneously. After the indicated times, the plates were briefly spun down and washed with PBS. Lysis reagent (20 μl per well) was then added. Luciferase Assay Reagent (100 μl per well) was added, and the plate was read using a GloMax Discover Microplate Reader (GM3000, Promega).

Generation of DR5 antibodies and comparison to DR5-scFv sEVs

DR5 monoclonal antibodies (tigatuzumab) were manufactured by Biointron Biological USA Inc. (Metuchen, NJ, USA). The number of antibody molecules was calculated using Avogadro's number and the molecular weight of tigatuzumab. Avogadro's number (6.022×10^{23} mol^{-1}) represents the number of molecules in one mole of a substance. Number of antibodies = Moles × Avogadro's number. sEV number was quantified using NTA.

Annexin V–7-AAD apoptosis assay

An apoptosis assay was performed using the FITC Annexin V Apoptosis Detection Kit with 7-AAD (640922, BioLegend). Briefly, cells were washed twice with cold Cell Staining Buffer and resuspended in Annexin V Binding Buffer at a concentration of 1×10^7/ml. Then, 100 μl of cell suspension was stained with 5 μl of FITC Annexin V and 5 μl of 7-AAD Viability Staining Solution and incubated for 15 min at room temperature in the dark. Annexin V Binding Buffer (400 μl) was added, and the samples were analyzed by LSRA flow cytometry.

Flow cytometry assay

The suspended cells were collected by centrifugation at 300*g* for 5 min. Tissue slices were digested with collagenase IV (240 μg/ml), hyaluronidase (HAase; 300 μg/ml), and deoxyribonuclease (DNase) (60 μg/ml) at 37°C for 30 min. The tissues were ground and rinsed with cell strainers (100 μm). Surface antibodies were stained for 30 min at 4°C in the dark, and intercellular staining was performed for 60 min after fixation and permeabilization. The sources of the antibodies are listed in table S1. Data were acquired on LSRA or A3 Lite flow cytometers (BD Biosciences, NJ, USA) and analyzed using FlowJo software (Tree Star, OR, USA). Flow cytometry for sEVs was performed following the protocol described by Fu *et al.* (*11*). Briefly, sEVs were incubated with 4-μm-diameter aldehyde/sulfate latex beads (A37304, Invitrogen, MA, USA) for 15 min and then rotated for 1 hour at room temperature. After centrifugation, the pellet was blocked with fetal calf serum (FCS) for 30 min and washed three times with PBS. Beads were then incubated with corresponding fluorescent antibodies for 1 hour, subjected to LSRA or A3 Lite flow cytometry, and analyzed with FlowJo software.

Western blot

Cells or sEVs were lysed in radioimmunoprecipitation assay (RIPA) buffer. A total of 20 to 50 μg of protein was processed for SDS-PAGE (polyacrylamide gel electrophoresis) and electroblotted onto polyvinylidene difluoride (PVDF) membranes (Millipore, MA, USA). Blots were blocked with 5% nonfat milk and incubated with the corresponding primary antibodies (table S1) and horseradish peroxidase (HRP)–conjugated secondary antibodies. Membranes were developed using enhanced chemiluminescence (ECL) detection reagents (Pierce, Thermo Scientific, MA, USA).

Confocal imaging

For cells treated with sEVs, samples were stained with PI (421301, BioLegend) for 15 min at 4°C and Hoechst 33342 (62249, Thermo Scientific, MA, USA) for 10 min at room temperature before analysis. For staining of sEVs, Deep Red dye (Cy5) (1:2000, Invitrogen, C10046) was added to sEVs and incubated at 37°C for 10 min. The sEVs were washed twice with PBS and pelleted using ExoQuick-TC. The stained cells and sEVs were analyzed using a Zeiss LSM 710 confocal microscope (Leica, Wetzlar, Germany).

For live imaging, 1×10^5 of A375-GFP cells were seeded in u-Dish 35-mm plates and cultured at 37°C and 5% CO_2 overnight. Then, 100 μg of DR5-scFv sEVs was added to u-Dish on day 2. Simultaneously, PI (1:10,000) and Hoechst (1:10,000) were added to the u-Dish. A Zeiss microscope was used to capture and record videos.

In situ hybridization

Formalin-fixed paraffin-embedded (FFPE) tissues were sectioned in 5-μm thickness. Sectioned tissues on slides were used for in situ hybridization to probe specific mRNA following the protocol of RNAscope 2.5 HD Reagent Kit-Red (ACDscope, 322350). Probes specific to DR5 were purchased from ACDscope (Hs-TNFRSF10B-C1,1048531-C1). Fast-Red was used to develop the positive probe

signal, which was also included in the kit. Representative bright-field images are captured under a microscope.

Immunohistochemistry

FFPE tissues were sectioned in 5-μm thickness. Slides were boiled for 10 min in 1 mM citrate buffer (w/v) with pH 6.0 for antigen retrieval. ImmPRESS Excel Amplified HRP Polymer Staining kit (Vector Laboratories; MP-7601) was used for immunohistochemical staining. Primary antibody against DR5 (Invitrogen, MA5-32693) was diluted 1:200 in phosphate buffered solution (PBST) buffer and incubated with slides overnight at 4°C. 3,3′-Diaminobenzidine (DAB) was used as chromogen (Vector Laboratories; MP-7601). Images were captured under a microscope.

Characterization of sEVs using immunoelectron microscopy

For immunoelectron microscopy, sEVs suspended in PBS were placed on formvar carbon-coated nickel grids, blocked, and incubated with $F(ab')_2$ Fragment Goat Anti-Human IgG, followed by incubation with gold-conjugated goat anti-biotin (electron microscopy–grade 10 nm) (25249, Electron Microscopy Sciences, PA, USA). Each staining step was followed by five PBS washes and 10 double-distilled water (ddH_2O) washes before contrast staining with 2% uranyl acetate. sEVs were visualized using a JEM-1011 transmission electron microscope. The sizes and concentrations of the sEVs were measured using NanoSight NS300 (Malvern Instruments, Malvern, UK).

Xenograft tumor models

A375, WM4625, MDA-MB-231, and Huh-7 cells were collected and washed with PBS, and 5×10^6 were resuspended in 100 μl of cold serum-free DMEM and injected subcutaneously into the right flank of 6- to 8-week-old athymic BALB/c female nude mice (Jackson Laboratory). Each group had five mice and was treated with the corresponding sEVs once the tumors were palpable, and the tumor size reached approximately 50 mm^3. Tumors were measured at indicated time points using a ruler, and tumor volumes were calculated using the formula length × width × height/2 (mm^3). Tumor tissues were harvested, fixed in 10% buffered formalin, embedded in paraffin, sectioned at a thickness of 5 μm, and subjected to immunohistochemical analysis. For mice bearing tumors on both sides, A375-$DR5^{WT}$ and A375-$DR5^{KO}$ cells with firefly luciferase (ffLUC) were collected and resuspended in 100 μl of cold serum-free DMEM at a density of 5×10^7/ml. Then, 100 μl of A375-$DR5^{WT}$ cells was injected subcutaneously into the right flank, and 100 μl of A375-$DR5^{KO}$ cells was injected into the left flank of 8-week-old NSG mice. According to the manufacturer's instructions, in vivo imaging was performed using IVIS Spectrum CT (PerkinElmer, MA, USA).

Statistical analysis

Statistical analyses were performed using GraphPad V.6.0 (Prism software package version). Data are presented as means ± SD, and significant differences were examined using paired Student's *t* test, one-way analysis of variance (ANOVA), and two-way ANOVA.

Study approval

PBMCs were collected from healthy donors through the Human Immunology Core at the University of Pennsylvania with informed consent and institutional review board (IRB) approval (protocol number 707906). Fresh melanoma tissues were obtained from patients undergoing surgery at the Hospital of the University of Pennsylvania (PA, USA) with informed consent and IRB approval (protocol number 703001). All animal procedures were approved by the Institutional Animal Care and Use Committee of the University of Pennsylvania and Wistar Institute.

Supplementary Materials

The PDF file includes:

Figs. S1 to S15
Table S1
Legend for movie S1

Other Supplementary Material for this manuscript includes the following:

Movie S1

REFERENCES AND NOTES

1. F. Marofi, R. Motavalli, V. A. Safonov, L. Thangavelu, A. V. Yumashev, M. Alexander, N. Shomali, M. S. Chartrand, Y. Pathak, M. Jarahian, S. Izadi, A. Hassanzadeh, N. Shirafkan, S. Tahmasebi, F. M. Khiavi, CAR T cells in solid tumors: Challenges and opportunities. *Stem Cell Res. Ther.* **12**, 81 (2021).
2. G. Guzman, M. R. Reed, K. Bielamowicz, B. Koss, A. Rodriguez, CAR-T therapies in solid tumors: Opportunities and challenges. *Curr. Oncol. Rep.* **25**, 479–489 (2023).
3. R. A. Morgan, J. C. Yang, M. Kitano, M. E. Dudley, C. M. Laurencot, S. A. Rosenberg, Case report of a serious adverse event following the administration of T cells transduced with a chimeric antigen receptor recognizing ERBB2. *Mol. Ther.* **18**, 843–851 (2010).
4. S. A. Richman, S. Nunez-Cruz, B. Moghimi, L. Z. Li, Z. T. Gershenson, Z. Mourelatos, D. M. Barrett, S. A. Grupp, M. C. Milone, High-affinity GD2-specific CAR T cells induce fatal encephalitis in a preclinical neuroblastoma model. *Cancer Immunol. Res.* **6**, 36–46 (2018).
5. L. M. Doyle, M. Z. Wang, Overview of extracellular vesicles, their origin, composition, purpose, and methods for exosome isolation and analysis. *Cells* **8**, 727 (2019).
6. L. El-Shennawy, A. D. Hoffmann, N. K. Dashzeveg, K. M. McAndrews, P. J. Mehl, D. Cornish, Z. Yu, V. L. Tokars, V. Nicolaescu, A. Tomatsidou, C. Mao, C. J. Felicelli, C. F. Tsai, C. Ostiguin, Y. Jia, L. Li, K. Furlong, J. Wysocki, X. Luo, C. F. Ruivo, D. Batlle, T. J. Hope, Y. Shen, Y. K. Chae, H. Zhang, V. S. LeBleu, T. Shi, S. Swaminathan, Y. Luo, D. Missiakas, G. C. Randall, A. R. Demonbreun, M. G. Ison, R. Kalluri, D. Fang, H. Liu, Circulating ACE2-expressing extracellular vesicles block broad strains of SARS-CoV-2. *Nat. Commun.* **13**, 405 (2022).
7. G. Kibria, E. K. Ramos, Y. Wan, D. R. Gius, H. Liu, Exosomes as a drug delivery system in cancer therapy: Potential and challenges. *Mol. Pharm.* **15**, 3625–3633 (2018).
8. C. H. Wu, J. Li, L. Li, J. Sun, M. Fabbri, A. S. Wayne, R. C. Seeger, A. Y. Jong, Extracellular vesicles derived from natural killer cells use multiple cytotoxic proteins and killing mechanisms to target cancer cells. *J Extracell. Vesicles* **8**, 1588538 (2019).
9. X. Wang, Y. Zhang, X. Mu, C. R. Tu, Y. Chung, S. W. Tsao, G. C. Chan, W. H. Leung, Y. L. Lau, Y. Liu, W. Tu, Exosomes derived from γδ-T cells synergize with radiotherapy and preserve antitumor activities against nasopharyngeal carcinoma in immunosuppressive microenvironment. *J. Immunother. Cancer* **10**, e003832 (2022).
10. Y. Enomoto, P. Li, L. M. Jenkins, D. Anastasakis, G. C. Lyons, M. Hafner, W. J. Leonard, Cytokine-enhanced cytolytic activity of exosomes from NK Cells. *Cancer Gene Ther.* **29**, 734–749 (2022).
11. W. Fu, C. Lei, S. Liu, Y. Cui, C. Wang, K. Qian, T. Li, Y. Shen, X. Fan, F. Lin, M. Ding, M. Pan, X. Ye, Y. Yang, S. Hu, CAR exosomes derived from effector CAR-T cells have potent antitumour effects and low toxicity. *Nat. Commun.* **10**, 4355 (2019).
12. P. Yang, X. Cao, H. Cai, P. Feng, X. Chen, Y. Zhu, Y. Yang, W. An, Y. Yang, J. Jie, The exosomes derived from CAR-T cell efficiently target mesothelin and reduce triple-negative breast cancer growth. *Cell. Immunol.* **360**, 104262 (2021).
13. Z. Nahacka, J. Svadlenka, M. Peterka, M. Ksandrova, S. Benesova, J. Neuzil, L. Andera, TRAIL induces apoptosis but not necroptosis in colorectal and pancreatic cancer cells preferentially via the TRAIL-R2/DR5 receptor. *Biochim. Biophys. Acta Mol. Cell. Res.* **1865**, 522–531 (2018).
14. A. Kazaana, E. Sano, S. Yoshimura, K. Makita, H. Hara, A. Yoshino, T. Ueda, Promotion of TRAIL/Apo2L-induced apoptosis by low-dose interferon-β in human malignant melanoma cells. *J. Cell. Physiol.* **234**, 13510–13524 (2019).
15. C. Zheng, D. Zhou, W. Li, Y. Duan, M. Xu, J. Liu, J. Cheng, Y. Xiao, H. Xiao, T. Gan, J. Liang, D. Zheng, L. Wang, S. Zhang, Therapeutic efficacy of a MMAE-based anti-DR5 drug conjugate Oba01 in preclinical models of pancreatic cancer. *Cell Death Dis.* **14**, 295 (2023).
16. M. Kundu, Y. E. Greer, J. L. Dine, S. Lipkowitz, Targeting TRAIL death receptors in triple-negative breast cancers: Challenges and strategies for cancer therapy. *Cells* **11**, 3717 (2022).
17. B. T. Wang, T. Kothambawala, L. Wang, T. J. Matthew, S. E. Calhoun, A. K. Saini, M. F. Kotturi, G. Hernandez, E. W. Humke, M. S. Peterson, A. M. Sinclair, B. A. Keyt, Multimeric anti-DR5 IgM agonist antibody IGM-8444 is a potent inducer of cancer cell apoptosis and

synergizes with chemotherapy and BCL-2 inhibitor ABT-199. *Mol. Cancer Ther.* **20**, 2483–2494 (2021).
18. T. Mondal, G. N. Shivange, R. G. Tihagam, E. Lyerly, M. Battista, D. Talwar, R. Mosavian, K. Urbanek, N. S. Rashid, J. C. Harrell, P. D. Bos, E. B. Stelow, M. S. Stack, S. Bhatnagar, J. Tushir-Singh, Unexpected PD-L1 immune evasion mechanism in TNBC, ovarian, and other solid tumors by DR5 agonist antibodies. *EMBO Mol. Med.* **13**, e12716 (2021).
19. S. Sharma, E. G. de Vries, J. R. Infante, C. N. Oldenhuis, J. A. Gietema, L. Yang, S. Bilic, K. Parker, M. Goldbrunner, J. W. Scott, H. A. Burris III, Safety, pharmacokinetics, and pharmacodynamics of the DR5 antibody LBY135 alone and in combination with capecitabine in patients with advanced solid tumors. *Invest. New Drugs* **32**, 135–144 (2014).
20. A. Forero-Torres, K. E. Varley, V. G. Abramson, Y. Li, C. Vaklavas, N. U. Lin, M. C. Liu, H. S. Rugo, R. Nanda, A. M. Storniolo, T. A. Traina, S. Patil, C. H. Van Poznak, J. R. Nangia, W. J. Irvin Jr., H. Krontiras, J. F. D. L. Santos, P. Haluska, W. Grizzle, R. M. Myers, A. C. Wolff, Translational Breast Cancer Research Consortium (TBCRC), TBCRC 019: A phase II trial of nanoparticle albumin-bound paclitaxel with or without the anti-death receptor 5 monoclonal antibody tigatuzumab in patients with triple-negative breast cancer. *Clin. Cancer Res.* **21**, 2722–2729 (2015).
21. G. A. Dominguez, T. Condamine, S. Mony, A. Hashimoto, F. Wang, Q. Liu, A. Forero, J. Bendell, R. Witt, N. Hockstein, P. Kumar, D. I. Gabrilovich, Selective targeting of myeloid-derived suppressor cells in cancer patients using DS-8273a, an agonistic TRAIL-R2 antibody. *Clin. Cancer Res.* **23**, 2942–2950 (2017).
22. G. Pietra, C. Vitale, D. Pende, A. Bertaina, F. Moretta, M. Falco, P. Vacca, E. Montaldo, C. Cantoni, M. C. Mingari, A. Moretta, F. Locatelli, L. Moretta, Human natural killer cells: News in the therapy of solid tumors and high-risk leukemias. *Cancer Immunol. Immunother.* **65**, 465–476 (2016).
23. Q. Zhang, H. Zhang, J. Ding, H. Liu, H. Li, H. Li, M. Lu, Y. Miao, L. Li, J. Zheng, Combination therapy with EpCAM-CAR-NK-92 cells and regorafenib against human colorectal cancer models. *J. Immunol. Res.* **2018**, 4263520 (2018).
24. G. Roex, D. Campillo-Davo, D. Flumens, P. A. G. Shaw, L. Krekelbergh, H. De Reu, Z. N. Berneman, E. Lion, S. Anguille, Two for one: Targeting BCMA and CD19 in B-cell malignancies with off-the-shelf dual-CAR NK-92 cells. *J. Transl. Med.* **20**, 124 (2022).
25. L. Zhu, S. Kalimuthu, P. Gangadaran, J. M. Oh, H. W. Lee, S. H. Baek, S. Y. Jeong, S. W. Lee, J. Lee, B. C. Ahn, Exosomes derived from natural killer cells exert therapeutic effect in melanoma. *Theranostics* **7**, 2732–2745 (2017).
26. E. Kokalaki, B. Ma, M. Ferrari, T. Grothier, W. Hazelton, S. Manzoor, E. Costu, J. Taylor, A. Bulek, S. Srivastava, I. Gannon, R. Jha, R. Gealy, L. Stanczuk, T. Rizou, M. Robson, M. El-Kholy, V. Baldan, M. Righi, J. Sillibourne, S. Thomas, S. Onuoha, S. Cordoba, M. Pule, Dual targeting of CD19 and CD22 against B-ALL using a novel high-sensitivity aCD22 CAR. *Mol. Ther.* **31**, 2089–2104 (2023).
27. R. C. Sterner, R. M. Sterner, CAR-T cell therapy: Current limitations and potential strategies. *Blood Cancer J.* **11**, 69 (2021).
28. J. E. Pullan, M. I. Confeld, J. K. Osborn, J. Kim, K. Sarkar, S. Mallik, Exosomes as drug carriers for cancer therapy. *Mol. Pharm.* **16**, 1789–1798 (2019).
29. Y. Liang, L. Duan, J. Lu, J. Xia, Engineering exosomes for targeted drug delivery. *Theranostics* **11**, 3183–3195 (2021).
30. L. Ou, H. Wang, H. Huang, Z. Zhou, Q. Lin, Y. Guo, T. Mitchell, A. C. Huang, G. Karakousis, L. Schuchter, R. Amaravadi, W. Guo, J. Salvino, M. Herlyn, X. Xu, Preclinical platforms to study therapeutic efficacy of human γδ T cells. *Clin. Transl. Med.* **12**, e814 (2022).
31. T. Condamine, V. Kumar, I. R. Ramachandran, J. I. Youn, E. Celis, N. Finnberg, W. S. El-Deiry, R. Winograd, R. H. Vonderheide, N. R. English, S. C. Knight, H. Yagita, J. C. McCaffrey, S. Antonia, N. Hockstein, R. Witt, G. Masters, T. Bauer, D. I. Gabrilovich, ER stress regulates myeloid-derived suppressor cell fate through TRAIL-R-mediated apoptosis. *J. Clin. Invest.* **124**, 2626–2639 (2014).
32. A. Martens, K. Wistuba-Hamprecht, M. Geukes Foppen, J. Yuan, M. A. Postow, P. Wong, E. Romano, A. Khammari, B. Dreno, M. Capone, P. A. Ascierto, A. M. Di Giacomo, M. Maio, B. Schilling, A. Sucker, D. Schadendorf, J. C. Hassel, T. K. Eigentler, P. Martus, J. D. Wolchok, C. Blank, G. Pawelec, C. Garbe, B. Weide, Baseline peripheral blood biomarkers associated with clinical outcome of advanced melanoma patients treated with ipilimumab. *Clin. Cancer Res.* **22**, 2908–2918 (2016).
33. H. L. Kenerson, K. M. Sullivan, K. P. Labadie, V. G. Pillarisetty, R. S. Yeung, Protocol for tissue slice cultures from human solid tumors to study therapeutic response. *STAR Protoc.* **2**, 100574 (2021).
34. R. O. Elliott, M. He, Unlocking the power of exosomes for crossing biological barriers in drug delivery. *Pharmaceutics* **13**, 122 (2021).
35. X. Zhang, X. Yuan, H. Shi, L. Wu, H. Qian, W. Xu, Exosomes in cancer: Small particle, big player. *J. Hematol. Oncol.* **8**, 83 (2015).
36. K. Newick, S. O'Brien, E. Moon, S. M. Albelda, CAR T cell therapy for solid tumors. *Annu. Rev. Med.* **68**, 139–152 (2017).
37. C. H. June, R. S. O'Connor, O. U. Kawalekar, S. Ghassemi, M. C. Milone, CAR T cell immunotherapy for human cancer. *Science* **359**, 1361–1365 (2018).
38. C. H. June, M. Sadelain, Chimeric antigen receptor therapy. *N. Engl. J. Med.* **379**, 64–73 (2018).
39. C. L. Bonifant, H. J. Jackson, R. J. Brentjens, K. J. Curran, Toxicity and management in CAR T-cell therapy. *Mol. Ther. Oncolytics* **3**, 16011 (2016).
40. G. H. Nam, Y. Choi, G. B. Kim, S. Kim, S. A. Kim, I.-S. Kim, Emerging prospects of exosomes for cancer treatment: From conventional therapy to immunotherapy. *Adv. Mater.* **32**, e2002440 (2020).
41. B. Besse, M. Charrier, V. Lapierre, E. Dansin, O. Lantz, D. Planchard, T. Le Chevalier, A. Livartoski, F. Barlesi, A. Laplanche, S. Ploix, N. Vimond, I. Peguillet, C. Thery, L. Lacroix, I. Zoernig, K. Dhodapkar, M. Dhodapkar, S. Viaud, J. C. Soria, K. S. Reiners, E. Pogge von Strandmann, F. Vely, S. Rusakiewicz, A. Eggermont, J. M. Pitt, L. Zitvogel, N. Chaput, Dendritic cell-derived exosomes as maintenance immunotherapy after first line chemotherapy in NSCLC. *Oncoimmunology* **5**, e1071008 (2016).
42. K. Zhang, K. Cheng, Stem cell-derived exosome versus stem cell therapy. *Nat. Rev. Bioeng.* **1**, 608–609 (2023).
43. F. Korell, M. L. Schubert, T. Sauer, A. Schmitt, P. Derigs, T. F. Weber, P. Schnitzler, C. Muller-Tidow, P. Dreger, M. Schmitt, Infection complications after lymphodepletion and dosing of chimeric antigen receptor T (CAR-T) cell therapy in patients with relapsed/refractory acute lymphoblastic leukemia or B cell non-Hodgkin lymphoma. *Cancers* **13**, 1684 (2021).
44. L. Zhu, S. Kalimuthu, J. M. Oh, P. Gangadaran, S. H. Baek, S. Y. Jeong, S. W. Lee, J. Lee, B. C. Ahn, Enhancement of antitumor potency of extracellular vesicles derived from natural killer cells by IL-15 priming. *Biomaterials* **190-191**, 38–50 (2019).
45. S. Gurung, D. Perocheau, L. Touramanidou, J. Baruteau, The exosome journey: From biogenesis to uptake and intracellular signalling. *Cell Commun. Signal* **19**, 47 (2021).
46. A. Longatti, C. Schindler, A. Collinson, L. Jenkinson, C. Matthews, L. Fitzpatrick, M. Blundy, R. Minter, T. Vaughan, M. Shaw, N. Tigue, High affinity single-chain variable fragments are specific and versatile targeting motifs for extracellular vesicles. *Nanoscale* **10**, 14230–14244 (2018).
47. S. Ohno, M. Takanashi, K. Sudo, S. Ueda, A. Ishikawa, N. Matsuyama, K. Fujita, T. Mizutani, T. Ohgi, T. Ochiya, N. Gotoh, M. Kuroda, Systemically injected exosomes targeted to EGFR deliver antitumor microRNA to breast cancer cells. *Mol. Ther.* **21**, 185–191 (2013).
48. K. De Veirman, E. Van Valckenborgh, Q. Lahmar, X. Geeraerts, E. De Bruyne, E. Menu, I. Van Riet, K. Vanderkerken, J. A. Van Ginderachter, Myeloid-derived suppressor cells as therapeutic target in hematological malignancies. *Front. Oncol.* **4**, 349 (2014).
49. M. Dall'Ora, G. Rovesti, L. Reggiani Bonetti, G. Casari, F. Banchelli, L. Fabbiani, E. Veronesi, T. Petrachi, P. Magistri, F. Di Benedetto, A. Spallanzani, C. Chiavelli, M. C. Spano, A. Maiorana, M. Dominici, G. Grisendi, TRAIL receptors are expressed in both malignant and stromal cells in pancreatic ductal adenocarcinoma. *Am. J. Cancer Res.* **11**, 4500–4514 (2021).
50. A. Hazrati, S. Soudi, K. Malekpour, M. Mahmoudi, A. Rahimi, S. M. Hashemi, R. S. Varma, Immune cells-derived exosomes function as a double-edged sword: Role in disease progression and their therapeutic applications. *Biomark. Res.* **10**, 30 (2022).
51. F. Wu, M. Xie, M. Hun, Z. She, C. Li, S. Luo, X. Chen, W. Wan, C. Wen, J. Tian, Natural killer cell-derived extracellular vesicles: Novel players in cancer immunotherapy. *Front. Immunol.* **12**, 658698 (2021).
52. I. Rahimmanesh, M. Totonchi, H. Khanahmad, The challenging nature of primary T lymphocytes for transfection: Effect of protamine sulfate on the transfection efficiency of chemical transfection reagents. *Res. Pharm. Sci.* **15**, 437–446 (2020).
53. W. Hu, G. Wang, D. Huang, M. Sui, Y. Xu, Cancer immunotherapy based on natural killer cells: Current progress and new opportunities. *Front. Immunol.* **10**, 1205 (2019).
54. J. Wang, E. E. Bonacquisti, A. D. Brown, J. Nguyen, Boosting the biogenesis and secretion of mesenchymal stem cell-derived exosomes. *Cells* **9**, 660 (2020).
55. K. W. Witwer, B. W. M. Van Balkom, S. Bruno, A. Choo, M. Dominici, M. Gimona, A. F. Hill, D. De Kleijn, M. Koh, R. C. Lai, S. A. Mitsialis, L. A. Ortiz, E. Rohde, T. Asada, W. S. Toh, D. J. Weiss, L. Zheng, B. Giebel, S. K. Lim, Defining mesenchymal stromal cell (MSC)-derived small extracellular vesicles for therapeutic applications. *J. Extracell. Vesicles* **8**, 1609206 (2019).
56. C. Théry, K. W. Witwer, E. Aikawa, M. J. Alcaraz, J. D. Anderson, R. Andriantsitohaina, A. Antoniou, T. Arab, F. Archer, G. K. Atkin-Smith, D. C. Ayre, J.-M. Bach, D. Bachurski, H. Baharvand, L. Balaj, S. Baldacchino, N. N. Bauer, A. A. Baxter, M. Bebawy, C. Beckham, A. B. Zavec, A. Benmoussa, A. C. Berardi, P. Bergese, E. Bielska, C. Blenkiron, S. Bobis-Wozowicz, E. Boilard, W. Boireau, A. Bongiovanni, F. E. Borràs, S. Bosch, C. M. Boulanger, X. Breakefield, A. M. Breglio, M. Á. Brennan, D. R. Brigstock, A. Brisson, M. L. Broekman, J. F. Bromberg, P. Bryl-Górecka, S. Buch, A. H. Buck, D. Burger, S. Busatto, D. Buschmann, B. Bussolati, E. I. Buzás, J. B. Byrd, G. Camussi, D. R. Carter, S. Caruso, L. W. Chamley, Y.-T. Chang, C. Chen, S. Chen, L. Cheng, A. R. Chin, A. Clayton, S. P. Clerici, A. Cocks, E. Cocucci, R. J. Coffey, A. Cordeiro-da-Silva, Y. Couch, F. A. Coumans, B. Coyle, R. Crescitelli, M. F. Criado, C. D'Souza-Schorey, S. Das, A. D. Chaudhuri, P. de Candia, E. F. De Santana, O. De Wever, H. A. Del Portillo, T. Demaret, S. Deville, A. Devitt, B. Dhondt, D. D. Vizio, L. C. Dieterich, V. Dolo, A. P. D. Rubio, M. Dominici, M. R. Dourado, T. A. Driedonks, F. V. Duarte, H. M. Duncan, R. M. Eichenberger, K. Ekström,

S. E. Andaloussi, C. Elie-Caille, U. Erdbrügger, J. M. Falcón-Pérez, F. Fatima, J. E. Fish, M. Flores-Bellver, A. Försönits, A. Frelet-Barrand, F. Fricke, G. Fuhrmann, S. Gabrielsson, A. Gámez-Valero, C. Gardiner, K. Gärtner, R. Gaudin, Y. S. Gho, B. Giebel, C. Gilbert, M. Gimona, I. Giusti, D. C. Goberdhan, A. Görgens, S. M. Gorski, D. W. Greening, J. C. Gross, A. Gualerzi, G. N. Gupta, D. Gustafson, A. Handberg, R. A. Haraszti, P. Harrison, H. Hegyesi, A. Hendrix, A. F. Hill, F. H. Hochberg, K. F. Hoffmann, B. Holder, H. Holthofer, B. Hosseinkhani, G. Hu, Y. Huang, V. Huber, S. Hunt, A. G.-E. Ibrahim, T. Ikezu, J. M. Inal, M. Isin, A. Ivanova, H. K. Jackson, S. Jacobsen, S. M. Jay, M. Jayachandran, G. Jenster, L. Jiang, S. M. Johnson, J. C. Jones, A. Jong, T. Jovanovic-Talisman, S. Jung, R. Kalluri, S.-I. Kano, S. Kaur, Y. Kawamura, E. T. Keller, D. Khamari, E. Khomyakova, A. Khvorova, P. Kierulf, K. P. Kim, T. Kislinger, M. Klingeborn, D. J. Klinke II, M. Kornek, M. M. Kosanović, Á. F. Kovács, E.-M. Krämer-Albers, S. Krasemann, M. Krause, I. V. Kurochkin, G. D. Kusuma, S. Kuypers, S. Laitinen, S. M. Langevin, L. R. Languino, J. Lannigan, C. Lässer, L. C. Laurent, G. Lavieu, E. Lázaro-Ibáñez, S. L. Lay, M.-S. Lee, Y. X. F. Lee, D. S. Lemos, M. Lenassi, A. Leszczynska, I. T. Li, K. Liao, S. F. Libregts, E. Ligeti, R. Lim, S. K. Lim, A. Linē, K. Linnemannstöns, A. Llorente, C. A. Lombard, M. J. Lorenowicz, Á. M. Lörincz, J. Lötvall, J. Lovett, M. C. Lowry, X. Loyer, Q. Lu, B. Lukomska, T. R. Lunavat, S. L. Maas, H. Malhi, A. Marcilla, J. Mariani, J. Mariscal, E. S. Martens-Uzunova, L. Martin-Jaular, M. C. Martinez, V. R. Martins, M. Mathieu, S. Mathivanan, M. Maugeri, L. K. M. Ginnis, M. J. M. Vey, D. G. Meckes Jr., K. L. Meehan, I. Mertens, V. R. Minciacchi, A. Möller, M. M. Jørgensen, A. Morales-Kastresana, J. Morhayim, F. Mullier, M. Muraca, L. Musante, V. Mussack, D. C. Muth, K. H. Myburgh, T. Najrana, M. Nawaz, I. Nazarenko, P. Nejsum, C. Neri, T. Neri, R. Nieuwland, L. Nimrichter, J. P. Nolan, E. N. N. Hoen, N. N. Hooten, L. O'Driscoll, T. O'Grady, A. O'Loghlen, T. Ochiya, M. Olivier, A. Ortiz, L. A. Ortiz, X. Osteikoetxea, O. Østergaard, M. Ostrowski, J. Park, D. M. Pegtel, H. Peinado, F. Perut, M. W. Pfaffl, D. G. Phinney, B. C. Pieters, R. C. Pink, D. S. Pisetsky, E. P. von Strandmann, I. Polakovicova, I. K. Poon, B. H. Powell, I. Prada, L. Pulliam, P. Quesenberry, A. Radeghieri, R. L. Raffai, S. Raimondo, J. Rak, M. I. Ramirez, G. Raposo, M. S. Rayyan, N. Regev-Rudzki, F. L. Ricklefs, P. D. Robbins, D. D. Roberts, S. C. Rodrigues, E. Rohde, S. Rome, K. M. Rouschop, A. Rughetti, A. E. Russell, P. Saá, S. Sahoo, E. Salas-Huenuleo, C. Sánchez, J. A. Saugstad, M. J. Saul, R. M. Schiffelers, R. Schneider, T. H. Schøyen, A. Scott, E. Shahaj, S. Sharma, O. Shatnyeva, F. Shekari, G. V. Shelke, A. K. Shetty, K. Shiba, P. R.-M. Siljander, A. M. Silva, A. Skowronek, O. L. Snyder II, R. P. Soares, B. W. Sódar, C. Soekmadji, J. Sotillo, P. D. Stahl, W. Stoorvogel, S. L. Stott, E. F. Strasser, S. Swift, H. Tahara, M. Tewari, K. Timms, S. Tiwari, R. Tixeira, M. Tkach, W. S. Toh, R. Tomasini, A. C. Torrecilhas, J. P. Tosar, V. Toxavidis, L. Urbanelli, P. Vader, B. W. van Balkom, S. G. van der Grein, J. Van Deun, M. J. van Herwijnen, K. Van Keuren-Jensen, G. van Niel, M. E. van Royen, A. J. van Wijnen, M. H. Vasconcelos, I. J. Vechetti Jr., T. D. Veit, L. J. Vella, É. Velot, F. J. Verweij, B. Vestad, J. L. Viñas, T. Visnovitz, K. V. Vukman, J. Wahlgren, D. C. Watson, M. H. Wauben, A. Weaver, J. P. Webber, V. Weber, A. M. Wehman, D. J. Weiss, J. A. Welsh, S. Wendt, A. M. Wheelock, Z. Wiener, L. Witte, J. Wolfram, A. Xagorari, P. Xander, J. Xu, X. Yan, M. Yáñez-Mó, H. Yin, Y. Yuana, V. Zappulli, J. Zarubova, V. Žėkas, J.-Y. Zhang, Z. Zhao, L. Zheng, A. R. Zheutlin, A. M. Zickler, P. Zimmermann, A. M. Zivkovic, D. Zocco, E. K. Zuba-Surma, Minimal information for studies of extracellular vesicles 2018 (MISEV2018): A position statement of the International Society for Extracellular Vesicles and update of the MISEV2014 guidelines. *J. Extracell. Vesicles* **7**, 1535750 (2018).

57. S. Gandham, X. Su, J. Wood, A. L. Nocera, S. C. Alli, L. Milane, A. Zimmerman, M. Amiji, A. R. Ivanov, Technologies and standardization in research on extracellular vesicles. *Trends Biotechnol.* **38**, 1066–1098 (2020).
58. A. Stawarska, M. Bamburowicz-Klimkowska, E. Runden-Pran, M. Dusinska, M. R. Cimpan, I. Rios-Mondragon, I. P. Grudzinski, Extracellular vesicles as next-generation diagnostics and advanced therapy medicinal products. *Int. J. Mol. Sci.* **25**, 6533 (2024).
59. G. Chen, A. C. Huang, W. Zhang, G. Zhang, M. Wu, W. Xu, Z. Yu, J. Yang, B. Wang, H. Sun, H. Xia, Q. Man, W. Zhong, L. F. Antelo, B. Wu, X. Xiong, X. Liu, L. Guan, T. Li, S. Liu, R. Yang, Y. Lu, L. Dong, S. McGettigan, R. Somasundaram, R. Radhakrishnan, G. Mills, Y. Lu, J. Kim, Y. H. Chen, H. Dong, Y. Zhao, G. C. Karakousis, T. C. Mitchell, L. M. Schuchter, M. Herlyn, E. J. Wherry, X. Xu, W. Guo, Exosomal PD-L1 contributes to immunosuppression and is associated with anti-PD-1 response. *Nature* **560**, 382–386 (2018).

Acknowledgments: We would like to thank the volunteers who provided PBMC samples and all the patients who contributed samples to this work. **Funding:** This work was supported by NIH grants CA258113 (to X.X. and M.H.), CA261608 (to X.X., M.H., W.G., and R.A.), CA114046 (to X.X., M.H., and R.A.), CA284182 (to X.X.), and GM141832 (to W.G.). **Author contributions:** Conceptualization: X.X., T.M., Y.G., G.K., A.C.H., L.S., H.W., L.G., J.M., S.L., X.C., and R.A. Methodology: X.X., Y.G., L.H., Q.Z., H.W., L.G., J.M., S.L., Xia.Z., W.Z., and X.C. Investigation: J.Y., L.O., Y.G., Xin.Z., M.X., Q.Z., L.S., H.W., L.G., J.M., S.L., and X.C. Visualization: X.X., Y.G., W.G., A.C.H., L.G., S.L., and X.Z. Supervision: X.X. and L.G. Writing—original draft: X.X., Y.G., A.C.H., L.G., S.L., W.Z., and X.C. Writing—review and editing: X.X., T.M., Y.G., G.K., W.G., M.H., A.C.H., L.S., L.G., J.M., S.L., X.C., and R.A. Resources: X.X., T.M., G.K., M.X., H.M., Q.Z., L.S., H.W., L.G., J.M., S.L., Xia.Z., X.C., and A.F. Funding acquisition: X.X., L.G., and R.A. Validation: X.X., L.O., Y.G., Xin.Z., Xia.Z., Q.Z., H.W., L.G., S.L., Y.C., W.Z., and X.C. Formal analysis: P.G., X.X., Y.G., L.G., S.L., and Y.C. Supervision: X.X., T.M., L.S., L.G., X.C., and R.A. Project administration: X.X., T.M., L.S., H.W., L.G., S.L., and X.C. Data curation: S.L. and Y.C. Software: Y.C. and L.H. **Competing interests:** Y.G., H.W., X.Z., and X.X. are inventors on a patent application related to methods of DR5-scFv EV-based therapy (provisional patent) on behalf of the University of Pennsylvania. The provisional patent number is no. 63/702,481. TM received an honorarium for participating in the Scientific Advisory Board from Merck, BMS, and Pfizer. The other authors declare no competing interests. **Data and materials availability:** All data needed to evaluate the conclusions in the paper are present in the paper and/or the Supplementary Materials. DNA constructs can be provided by The Trustees of the University of Pennsylvania pending scientific review and a completed material transfer agreement. Requests for DNA constructs should be submitted to X.X. (xug@pennmedicne.upenn.edu).

Submitted 18 April 2024
Accepted 13 December 2024
Published 15 January 2025
10.1126/sciadv.adp9009